AD_____

Award Number: DAMD17-98-1-8511

TITLE: A Novel High Resolution Positron Emission Tomography System for Measurement of Bone Metabolism

PRINCIPAL INVESTIGATOR: John A. Correia, Ph.D.

CONTRACTING ORGANIZATION: Massachusetts General Hospital
Boston, Massachusetts 02114

REPORT DATE: September 1999

TYPE OF REPORT: Annual

PREPARED FOR: U.S. Army Medical Research and Materiel Command
Fort Detrick, Maryland 21702-5012

REPORT DOCUMENTATION PAGE

Form Approved
OMB No. 074-0188

1. AGENCY USE ONLY (Leave blank)	2. REPORT DATE	3. REPORT TYPE AND DATES COVERED
	September 1999	Annual (1 Sep 98 - 31 Aug 99)

4. TITLE AND SUBTITLE
A Novel High Resolution Positron Emission Tomography System for Measurement of Bone Metabolism

5. FUNDING NUMBERS
DAMD17-98-1-8511

6. AUTHOR(S)
John A. Correia, Ph.D.

7. PERFORMING ORGANIZATION NAME(S) AND ADDRESS(ES)
Massachusetts General Hospital
Boston, Massachusetts 02115

E-MAIL:

8. PERFORMING ORGANIZATION REPORT NUMBER

9. SPONSORING / MONITORING AGENCY NAME(S) AND ADDRESS(ES)
U.S. Army Medical Research and Materiel Command
Fort Detrick, Maryland 21702-5012

10. SPONSORING / MONITORING AGENCY REPORT NUMBER

11. SUPPLEMENTARY NOTES

12a. DISTRIBUTION / AVAILABILITY STATEMENT
Approved for public release; distribution unlimited

12b. DISTRIBUTION CODE

13. ABSTRACT ***(Maximum 200 Words)***

14. SUBJECT TERMS

15. NUMBER OF PAGES
41

16. PRICE CODE

17. SECURITY CLASSIFICATION OF REPORT	18. SECURITY CLASSIFICATION OF THIS PAGE	19. SECURITY CLASSIFICATION OF ABSTRACT	20. LIMITATION OF ABSTRACT
Unclassified	Unclassified	Unclassified	Unlimited

FOREWORD

Opinions, interpretations, conclusions and recommendations are those of the author and are not necessarily endorsed by the U.S. Army.

___ Where copyrighted material is quoted, permission has been obtained to use such material.

___ Where material from documents designated for limited distribution is quoted, permission has been obtained to use the material.

___ Citations of commercial organizations and trade names in this report do not constitute an official Department of Army endorsement or approval of the products or services of these organizations.

X In conducting research using animals, the investigator(s) adhered to the "Guide for the Care and Use of Laboratory Animals," prepared by the Committee on Care and use of Laboratory Animals of the Institute of Laboratory Resources, national Research Council (NIH Publication No. 86-23, Revised 1985).

N/A For the protection of human subjects, the investigator(s) adhered to policies of applicable Federal Law 45 CFR 46.

N/A In conducting research utilizing recombinant DNA technology, the investigator(s) adhered to current guidelines promulgated by the National Institutes of Health.

N/A In the conduct of research utilizing recombinant DNA, the investigator(s) adhered to the NIH Guidelines for Research Involving Recombinant DNA Molecules.

N/A In the conduct of research involving hazardous organisms, the investigator(s) adhered to the CDC-NIH Guide for Biosafety in Microbiological and Biomedical Laboratories.

PI - Signature 9/23/99 Date

TABLE OF CONTENTS:

I. - INTRODUCTION:

The overall purposes of this project are :

1. To design and develop an instrument for high resolution PET imaging of the long bones.
2. Demonstrate the use of this device in an experimental protocol to assess estrogen therapy for osteoporosis in a monkey model.

The main thrust of the first year's work was to carry out a design study for the proposed PET imaging device. Several approaches were used to accomplish this. First, a number of computational and simulation studies were done, secondly, a prototype device was constructed as a platform for testing circuit designs and data processing schemes, and finally the physical characteristics of the proposed design were evaluated using the prototype. Data acquisition and analysis software development have also been carried out using the prototype. A final design has been specified and ordering of components is in progress. The details of the work are described in the following sections and in the publications of Appendix I.

II. - REPORT BODY:

A. - Background:

PET (positron emission tomography) imaging is a nuclear medicine technique for measuring quantitative regional physiology and biochemistry in intact animals and humans. The penetrating radiation resulting from positron decay is in the form of two 511 keV photons which are time-correlated and leave the site of the decay in approximately opposite directions. PET imaging devices are designed to detect these photon-pairs as coincidence events. Detection of the photon pairs is the basis for the ability to fully correct for physical effects such as source self-absorption and photon scatter. Application of these corrections makes possible quantitative measurement radioactivity distributions. Large-scale PET devices (for human and large animal imaging) are highly evolved and commercially available. The frontier in PET imaging instrumentation lies in developing high resolution, small scale devices for imaging small animals or, in the case of this work, extremities. The advent of new

radiation-detector materials, particularly new scintillators such as Lutetium Orthosilicate (LSO), has made it possible to build such a small-scale device in practice.

The first year's work emphasized the design of an instrument for imaging primate extremities (and possibly human extremities in the future). The approach was to carry out simulation studies of physical and instrument factors as well as design and feasibility experiments in order to optimize the system design. Then a complete prototype instrument was constructed as an experimental platform for development of detector module designs, electronics, software for coincidence identification, and physical imaging studies. As a result a final configuration for the device proposed in this work has been established and construction has begun.

B. - Simulation Studies:

The parameters of importance in designing a small-scale PET instrument include detector diameter , detector element dimensions, shielding and coincidence-to-single-event ratio. These parameters determine the system sensitivity, resolution and count-rate capability.

The performance of small-scale single-plane PET geometries was studied using both Monte Carlo simulation and computation. The purpose of these studies was to characterize the expected performance of small diameter instruments. Effects taken into account in the simulations include: detailed properties of the radiation emission and interaction, detector array geometry, shielding geometry and detector material properties. The Monte Carlo studies were carried out in detail for the 12cm diameter prototype and for the 15cm diameter instrument which was initially proposed. Also, several other diameters were studied with a more limited subset of simulations. Studies were done at vertical detector openings (z) of 0.5 and 0.25cm. This parameter affects both the sensitivity and the z axis resolution. Lead (Pb) shielding with an imaging aperture of half the detector diameter was assumed. For each geometry, the diameter of a

cylindrical source of radioactivity and the detector energy thresholds were varied. Sample results for the 12cm diameter device are presented in figures 1a-1d. Figures 1a and 1b show the single event and coincidence event scatter fractions for 20 million coincidence events emitted from sources of various diameters. The fraction of scattered coincidences is typically very low (< 3% in the worst case of a 5cm diameter source) and agrees well with the experimental measurements discussed later. Figure 1c shows the single event-to-coincidence-event ratio as a function of source diameter, again for a total of 20 million events. Figure 1d, which incorporates the detector efficiency data of figure 3, shows the sensitivity of the instrument as a function of source diameter for 5mm deep LSO crystals. The data in figures 1a-1d are for a 125 keV energy threshold. Figures 2a-2d show similar results for a 15cm diameter detector. It should be noted that the sensitivity data of figure 2d, again incorporating the efficiency data of figure 3, is for 5mm deep crystals and the curves would be shifted upward by a factor of approximately 2 for 7mm deep crystals. The coincidence scatter fraction is less than 2.5% for the worst case of a 7cm diameter source.

Conclusions from these studies are as follows: (1) results for the 12cm diameter prototype agree well experimental measurements from the prototype (2) A larger 15cm diameter device will perform acceptably for bone imaging (3) The geometies studied yield an acceptably low scattered coincidence fraction (4) The coincidence-event to single-event ratios, which affect system dead time, are acceptably low for the designs studied.

Monte Carlo simulations of detection efficiency for LSO and other materials and detector penetration effects for 1mm wide LSO detectors were also carried out to determine optimum crystal length. Figure 3 shows the results for LSO at three energy threshold levels. The prototype device was constructed using 5mm deep crystals and a 125 keV energy threshold to minimize multiple-interaction events within the detectors. This results in a single-event detector efficiency of approximately 25% at 125 keV threshold and a coincidence sensitivity (square of single detector efficiency) of approximately 6.3%. If the depth of the detectors was extended to 7mm the coincidence efficiency would be increased to approximately 12%.

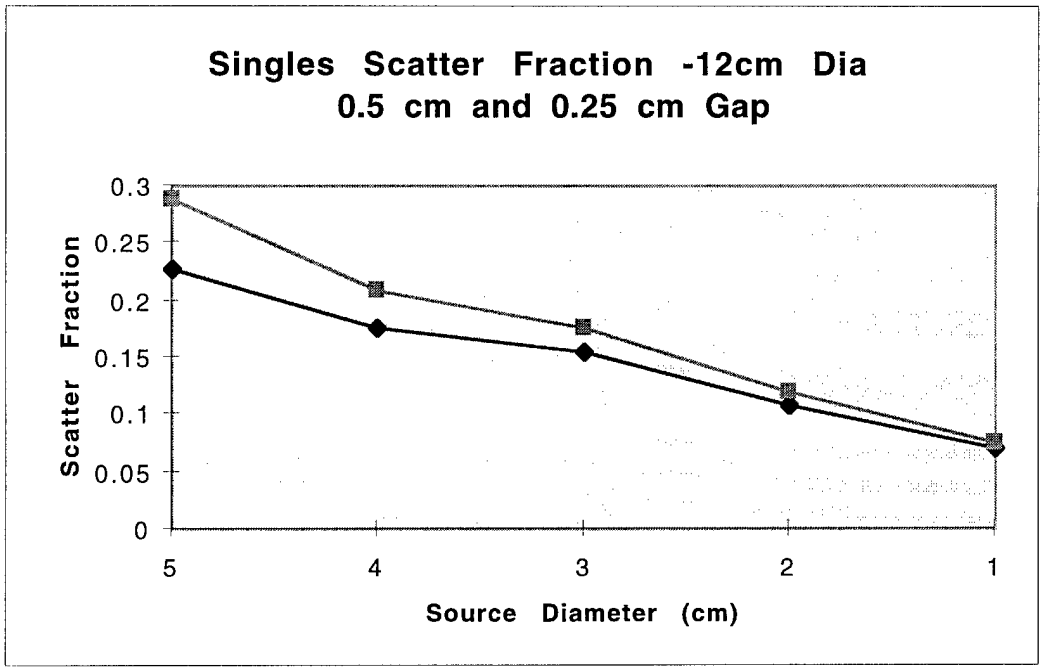

Figure 1a: Monte Carlo simulation of fraction of single events scattered for a 12cm diameter detector ring as a function of the diameter of a 10 cm long cylindrical source and a 6cm imaging aperture. Vertical (z) detector opening of 0.5 and 0.25 cm. 20 Million events simulated.

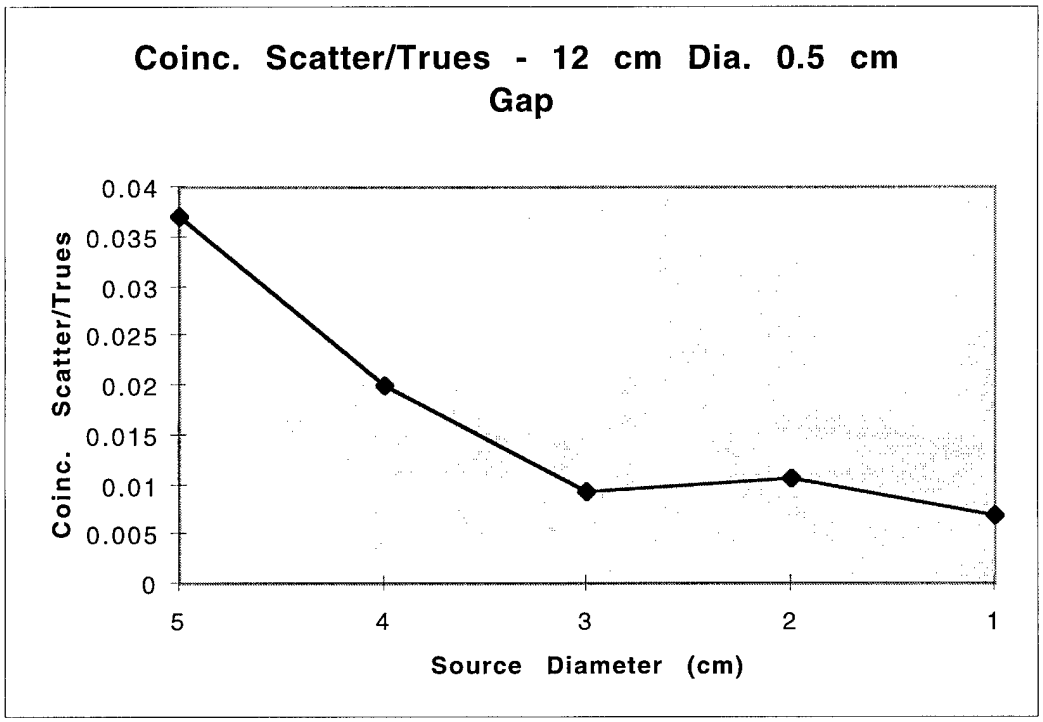

Figure 1b: Monte Carlo simulation of fraction of coincidence events scattered for a 12cm diameter detector ring as a function of the diameter of a 10cm long cylindrical source and a 6cm imaging aperture. Vertical (z) detector opening of 0.5 cm. 20 Million events simulated.

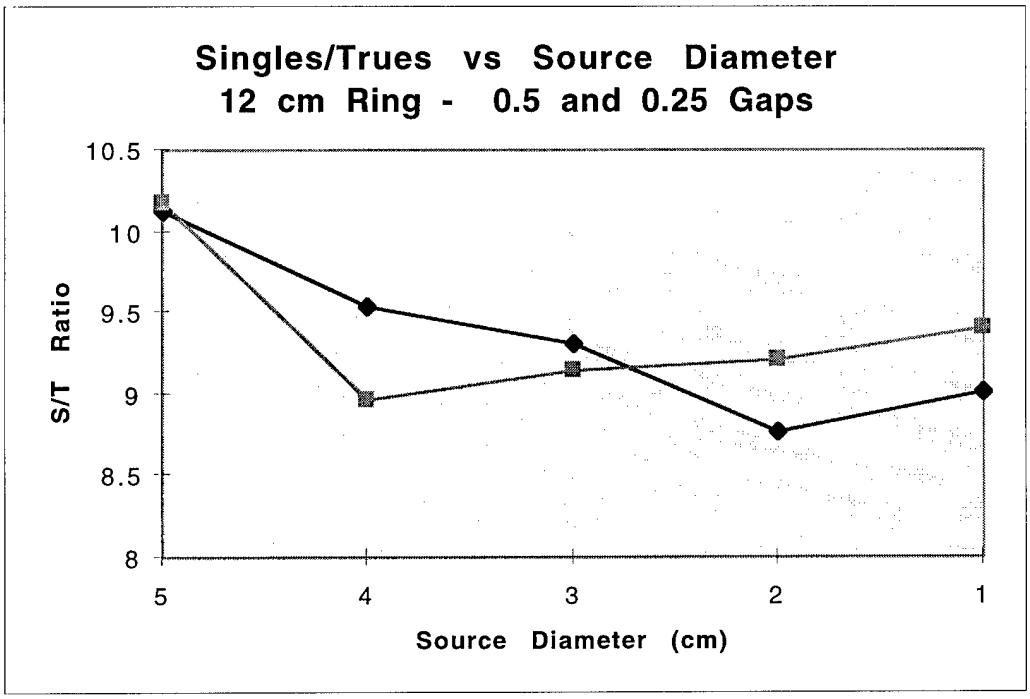

Figure 1c: Monte Carlo simulation of fraction of single/coincidence ratio for a 12cm diameter detector ring as a function of the diameter of a 10cm long cylindrical source and a 6cm imaging aperture. Vertical (z) detector opening of 0.5 and 0.25 cm. 20 Million events simulated.

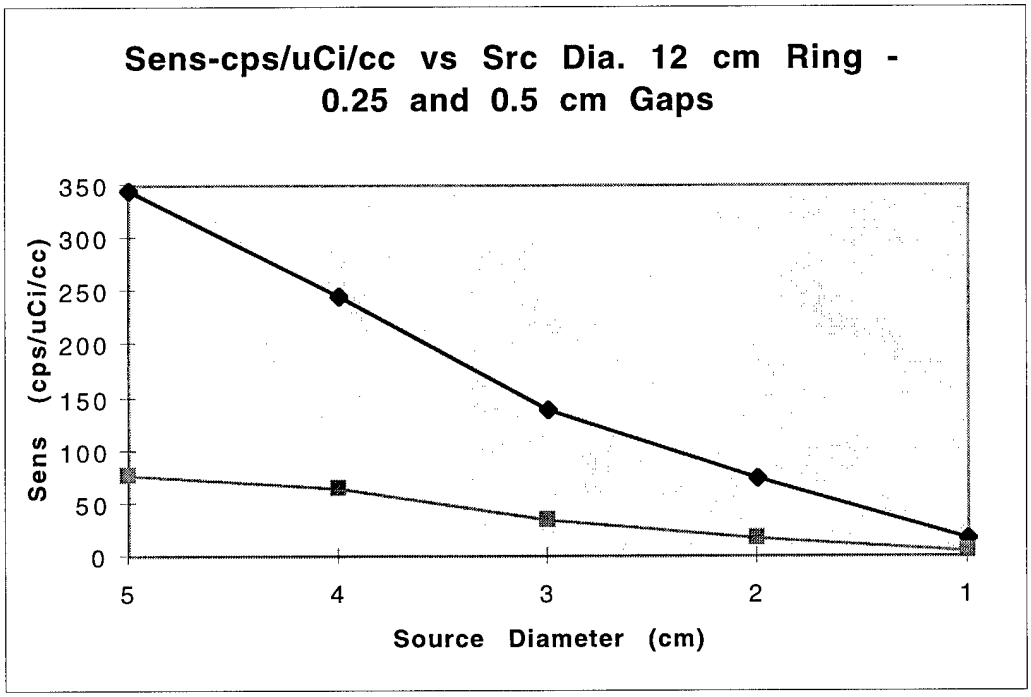

Figure 1d: Monte Carlo simulation of raw system sensitivity including detector efficiency for a 12 cm diameter detector ring as a function of the diameter for a 10 cm long cylindrical source and a 6cm imaging aperture. Vertical (z) detector opening of 0.5 and 0.25cm. 20 Million events simulated.

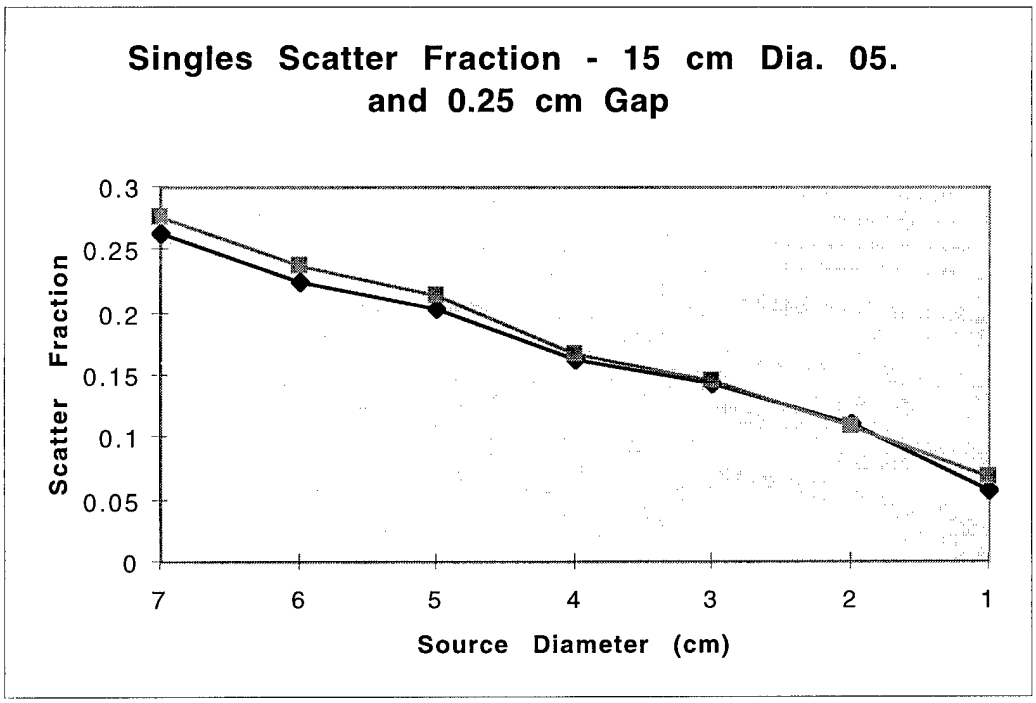

Figure 2a: Monte Carlo simulation of fraction of single events scattered for a 15cm diameter detector ring as a function of the diameter of a 10cm long cylindrical source and an 8cm imaging aperture. Vertical (z) detector opening of 0.5 and 0.25cm. 20 Million events simulated.

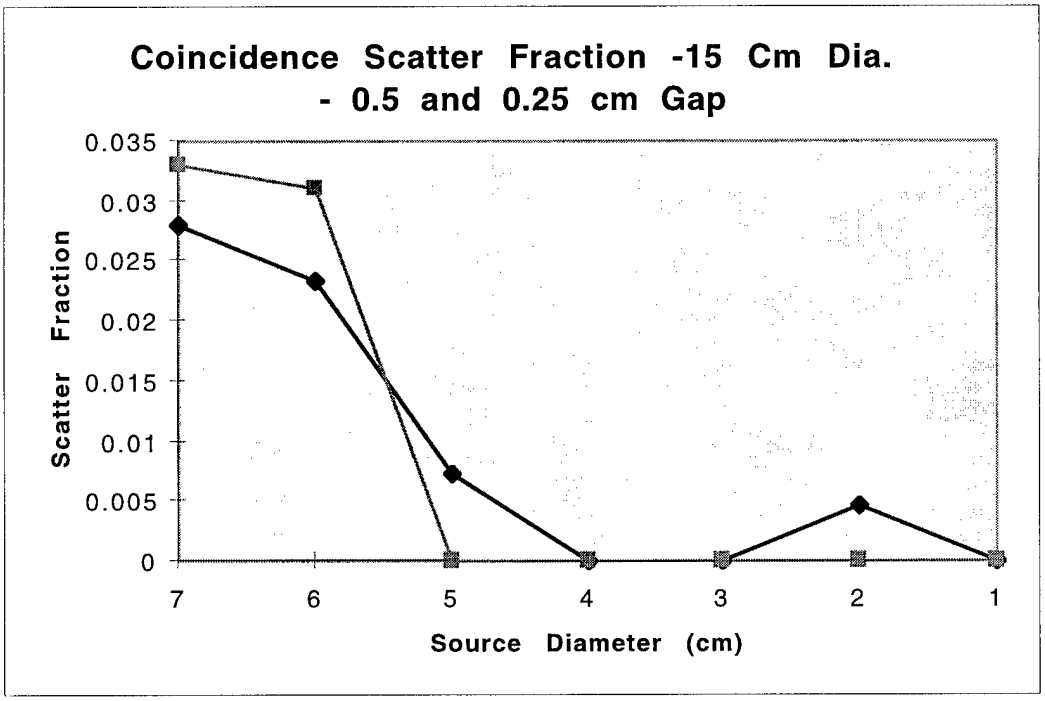

Figure 2b: Monte Carlo simulation of fraction of coincidence events scattered for a 15cm diameter detector ring as a function of the diameter of a 10cm long cylindrical source and an 8cm imaging aperture. Vertical (z) detector opening of 0.5 cm. 20 Million events simulated.

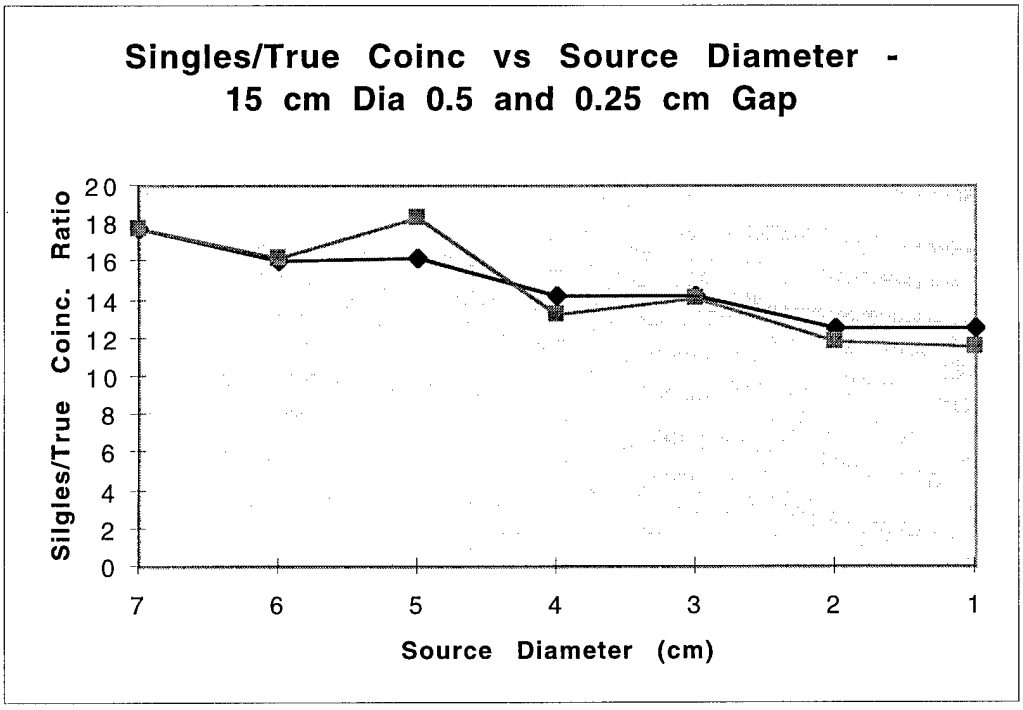

Figure 2c: Monte Carlo simulation of single/coincidence ratio for a 15cm diameter detector ring as a function of the diameter of a 10cm long cylindrical source and an 8cm imaging aperture. Vertical (z) detector opening of 0.5 and 0.25cm. 20 Million events simulated.

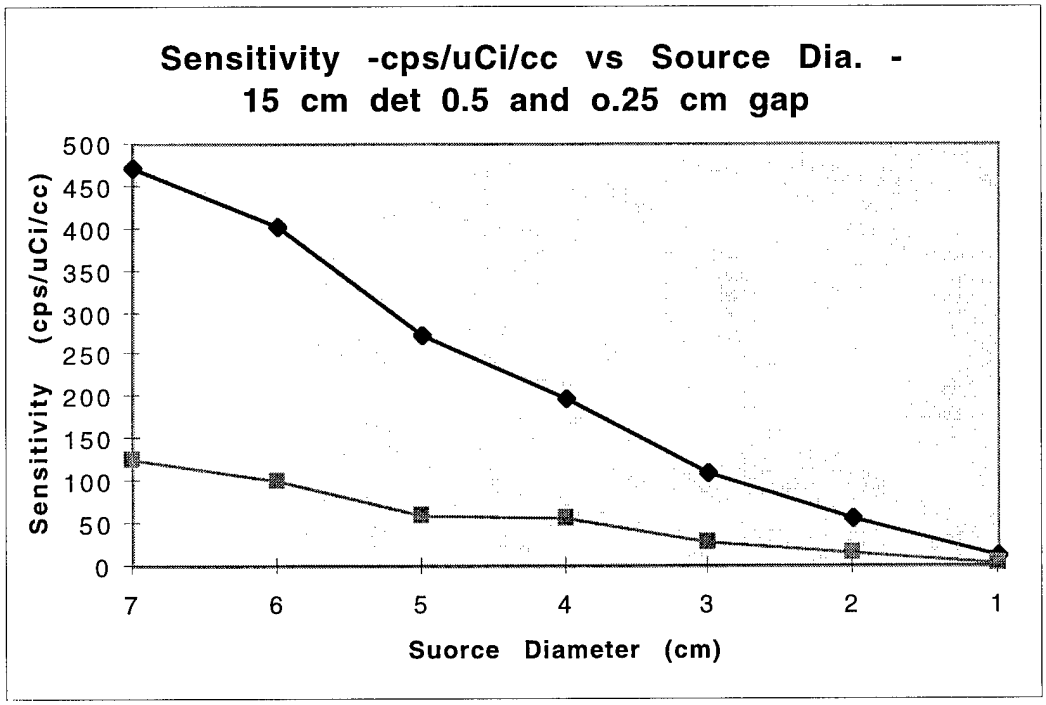

Figure 2d: Monte Carlo simulation raw system sensitivity including detector efficiency for a 15cm diameter detector ring as a function of the diameter of a 10cm long cylindrical source and an 8cm imaging aperture. Vertical (z) detector opening of 0.5 and 0.25cm. 20 Million events simulated.

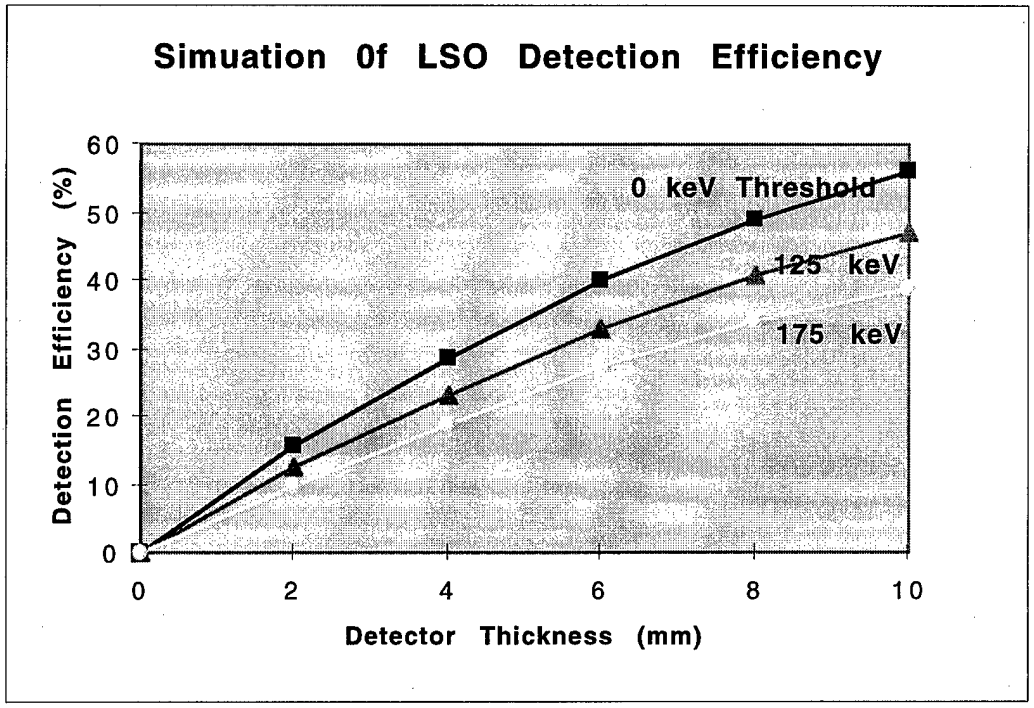

Figure 3: Monte Carlo simulation of 511 keV photon efficiency for LSO as a function of depth at several energy thresholds.

A major limitation to achieving high resolution is the penetration of photons into detector elements adjacent to the primary element when such photons are incident at angles other than 90 degrees. If longer detectors are used to increase efficiency the effect of this penetration becomes larger for a given detector-ring diameter. This is a major reason for choosing short detectors. Penetration effects were calculated for a series of detector diameters and crystal lengths. An example of the results is shown in figure 4 which presents a calculation of this penetration effect for 5mm thick detectors in the 12cm diameter detector ring. The experimental resolution measurements shown in a later section support the conclusion that this is a tractable effect, especially if objects imaged are limited to the central third of the field, and therefore correction for crystal penetration effect is not necessary. Since it is desirable that the final design have a larger diameter than the prototype to accoodate bigger objects, the same penetration effect was studied for a 15cm ring and 7mm deep detectors. A 7mm deep detector would result in a 12% coincidence efficiency (96% increase over a 5mm detector) while the resulting loss in overall instrument efficiency due

to an increase in diameter would be only 25%. The penetration curves for a 15 cm diameter and 7mm detectors are the same shape as those of figure 4 with the y axis increased to increased detector depth. It may be concluded that, if imaging is limited to the central third of the field no correction for penetration effects in a 15cm design is necessary.

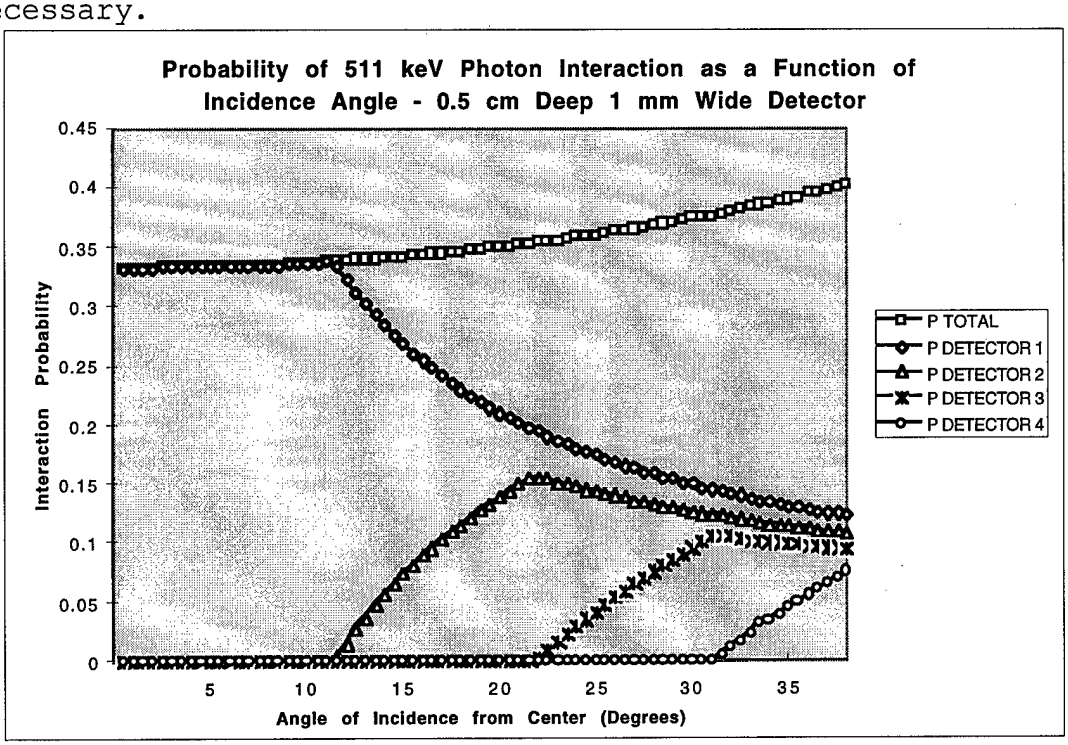

Figure 4: Detector penetration as a function of photon incidence angle for 1x4.5x5mm LSO detector array. The top curve shows total probability of interaction. The four lower curves represent, respectively the primary detector and each of the three adjacent detectors along the photon's geometric path. The central third of the detector field has a limiting incidence angle of 19 degrees. The same dataset for a 15 centimeter ring and 7mm deep detectors looks essentially the same with the y axis scaled up by approximately a factor of 1.5.

Based on the properties of the prototype and information from the literature concerning the behavior of fluorescent (non-radioactive) tetracycline compounds, calculations were carried our to determine if a reasonable PET signal would be obtained from a labeled tetracycline. This is an important issue since the thickness of the growth bands in primate long bones is quite small, on the order of 100u. The calculations use properties of fluorescent tetracycline kinetics from the literature and tissue radioactivity data from PET primate experiments at our laboratory. From the results, shown in figures 5a and 5b, it may be concluded that the measurement of bone growth rings in monkey long bones is feasible with reasonable injected doses of radioactivity (20-75 mCi). Although the signal is small, the high resolution of the imaging device will allow separation of the inner and outer

surfaces of the long bones and changes in growth rate with time on the order of 10% should be easily detectable in monkeys.

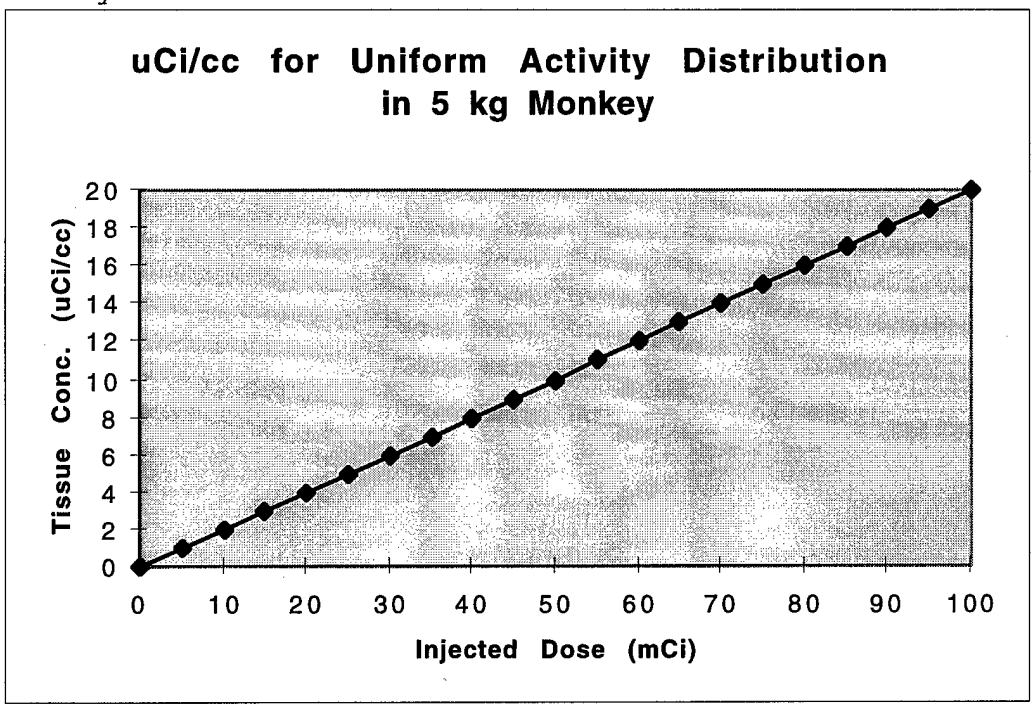

Figure 5a: Tissue radioactivity concentration in a 5kg monkey vs injected dose. Assumption of uniform radioactivity distribution is made.

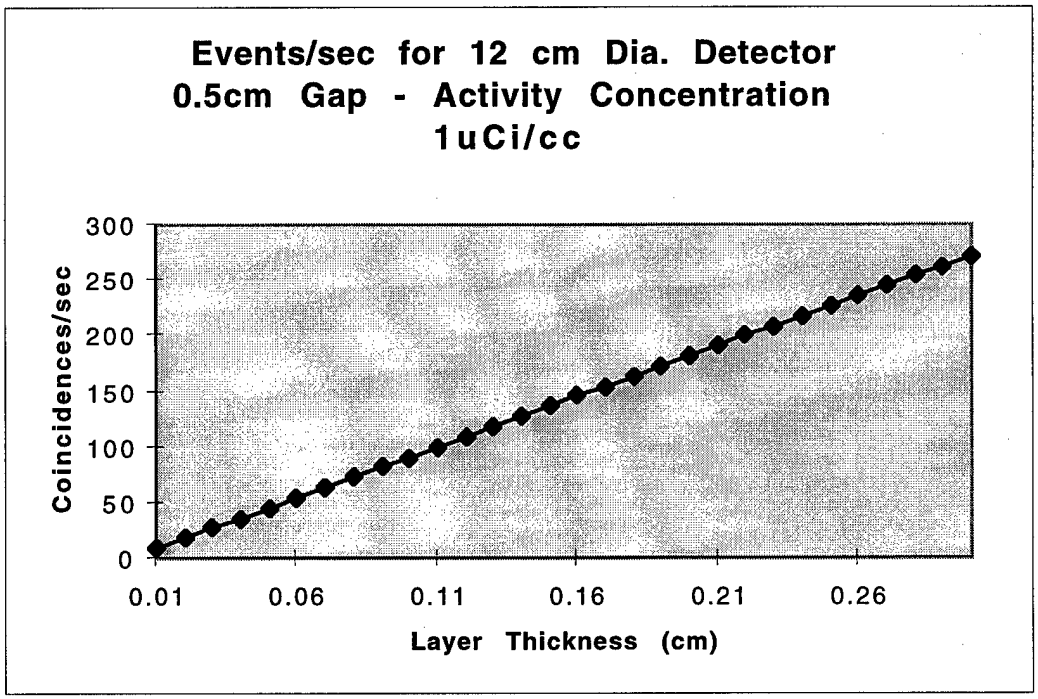

Figure 5b: The computed number of detected coincidence events per second for monkey long bone layers of various thicknesses having a concentration of 1 uCi/cc.

C - Design of Blocks and Electronics:

A schematic diagram of the prototype system is shown in figure 6. The detector array consists of a single ring of 360 1x4.5x5mm LSO crystals organized into blocks of 12 crystals each, viewed by two photomultiplier tubes (PMT's). The diameter of the detector array is 12cm. The 5mm deep crystals moderate the degradation and non-uniformity of resolution caused by multiple detector penetration at photon incidence angles far from the normal and minimize blurring due to multiple interaction sites. The choice of thin crystals represents a sacrifice in sensitivity to preserve resolution. The PMT signals are processed for timing and pulse height. The coincidence logic uses the timing signal to identify any coincidence event from the central volume of the detector. The 30 pulse-height signals are DC coupled to the sample-and-hold ADC. Pulse shaping equivalent to a single delay line clipping is used. When a coincidence event is detected the 30 signals are simultaneously sampled and converted to thirty 8 bit words. The deadtime is limited by the time required to transfer, process and store an event in the Computer. The preamplifiers, coincidence circuits and digital conversion circuits were implemented using standard logic elements. In the course of setting up the prototype a number of circuit board designs were generated. These included a PMT preamplifier, event processing boards, a coincidence circuit and a board which transfers coincidence data sets to a computer interface. All of these designs are functioning well in the prototype and will be used in the final instrument. The preamplifier layout has been changed to incorporate modifications made during development.

In the detector block, it is required that some fraction of the scintillation light from any crystal reach each the PMT's viewing that block. This requires that the surfaces of the crystals be treated in different ways depending on their position within the block. A number of different surface combinations were studied both by computer simulation of the light optics and by construction of prototype crystal blocks. Preliminary designs for both a 12 crystal block with 1mm resolution and a 10 crystal block with 1.2mm resolution were established and test-blocks evaluated. Based on the results

of these studies a set of 30 12-crystal blocks were constructed in an attempt to achieve 1mm instrument resolution. As will be mentioned below, the prototype ultimately achieved 1.2mm resolution due to limitations in the performance of the blocks. It was therefore decided to construct the final system to a specification of 1.2mm resolution using 1.2mm crystals.

To fabricate the blocks, the eight interior crystal faces were glued together in a jig with an 8° taper in order to point them toward the ring center. The next two on each side were separated from the central crystals and each other by an air gap. The two outside crystals have polished surfaces and a partial reflector isolates them from the adjacent crystals. A full reflector is used between blocks. Benchtop measurements have established that approximately 1/3 of the light from the peak signals is lost and the energy resolution of the blocks at 511 keV is 17%. A diagram of the 12 crystal block is shown in figure 7. A major technical accomplishment of the project was the development of a method for fabricating the blocks.

A simple ISA-bus-based data acquisition interface was constructed to acquire test data from the prototype system. Based on the experience gained with this interface, a number of commercially available PCI-Bus-based data acquisition interfaces were evaluated and the one most suited to our situation was chosen. This acquisition interface is now in-house along with a new computer system and we have begun to develop software for its use.

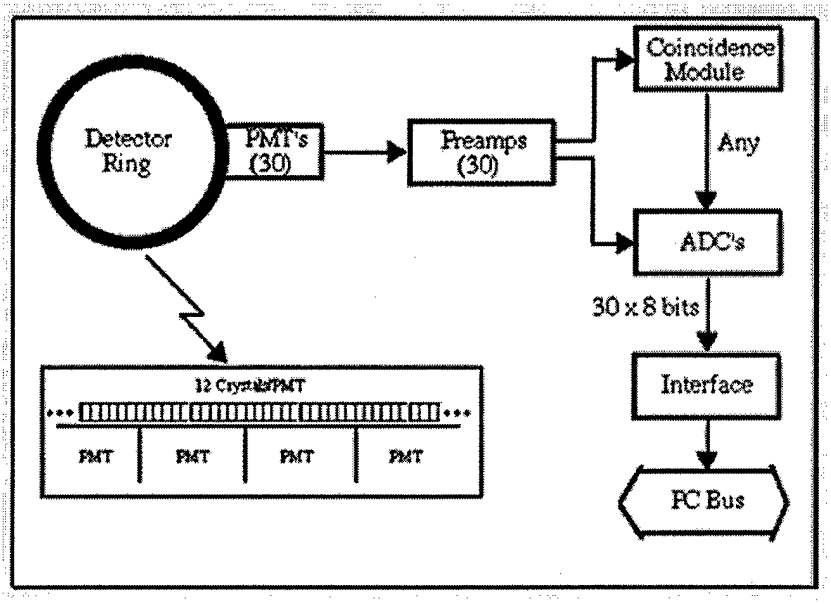

Figure 6: Prototype system diagram showing data acquisition front end electronics.

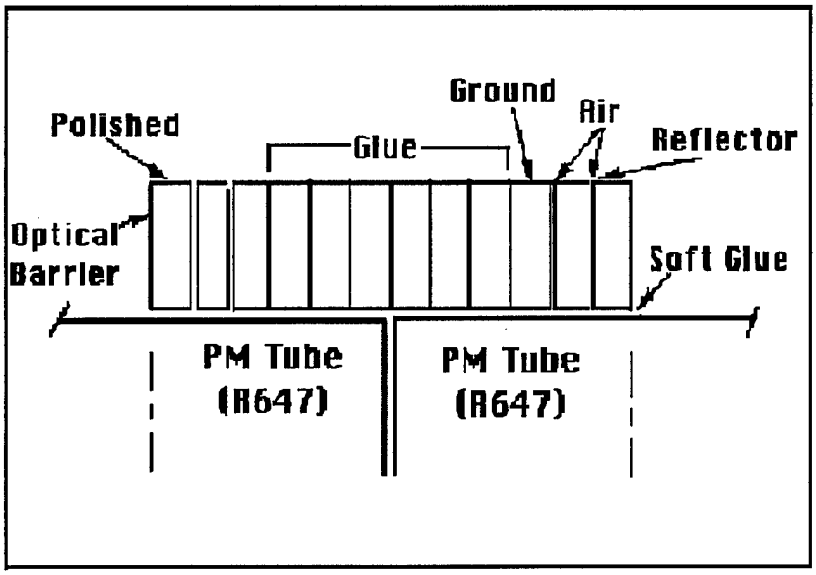

Figure 7: Diagram of LSO 12 crystal block attached to two photomultiplier tubes. Various surface preparations for light distribution are shown.

D. - Design of Data Processing Scheme:

Each block of twelve crystals is viewed by two adjacent PMT's. Signals from these PMT's, which are proportional to the light reaching each, are used to compute the identity the crystal in which a given event originated. The details this computation are as follows. Once a coincidence event is registered by the hardware and the 30 PMT signals are transferred to the computer. The sum of neighboring pairs of PMT signals is computed. When a sum exceeds both neighboring sums and an energy threshold, a block is identified. When exactly two blocks are identified within a data set the processing proceeds to the identification of the individual crystals within each. The normalized difference (**R**) of photomultipler signals (**A** and **B**) in each block is determined as follows:

(1) $$R = (A - kB) / (A + kB)$$

and if an energy criterion to select only events about the photopeak:

(2) $$E > E_{threshold} \quad \text{and} \quad E_{lower} < E < E_{upper}$$

is met, a particular crystal is identified, otherwise the event is rejected.

A given value of **R** is associated with an individual crystal within the block via a lookup table specifying the lower and upper levels of the ratio values for that crystal. A good event is recorded if the boundary conditions are met and the PMT-sum, or total energy, signal is within a window derived from the crystal energy spectra. Boundary and energy lookup tables are specified for each block to account for small variations in crystal properties and alignment among blocks. In addition a third block specific lookup table (**k** in equation 1) is used to normalize the **R** spectrum to zero at the center of each block. The determination of the lookup tables is an iterative process in which a starting set of boundaries are specified from **R** plots with wide energy windows, then a set of narrower energy windows are specified from the energy spectra and the process repeated until an optimum is reached. Figures 8 and 9 show a normalized difference spectrum and crystal energy spectra, respectively, from a typical block. It should be noted that the separation of the end crystals is less complete than those at the

center. The above described algorithm and tuning method have been extensively tested in the prototype.

Coincidence data are mapped to a sinogram format for storage. The sinogram format is a histogram of events as a function of field radius and angular position. It is a representation which is convenient for image reconstruction and has been used in most earlier PET scanners. The sinogram is subsequently corrected for sensitivity and reconstructed using a standard convolution-back-projection algorithm.

From the studies carried out with the prototype blocks it was concluded that the maximum system resolution of 1mm was not achieved due do several factors including limitations of light collection from the crystals, small imprecisions in the alignment of crystals within the blocks, relatively poor energy resolution near the center of the , and limitations of the original preamplifier design. Based on these results we have redesigned the preamplifier and have made the decision that the final instrument will be constructed with 1.2mm crystals yielding a system resolution of 1.2mm with considerably better block performance. All other circuit components designed for the prototype system have functioned well and therefore the same designs will be used in the final system.

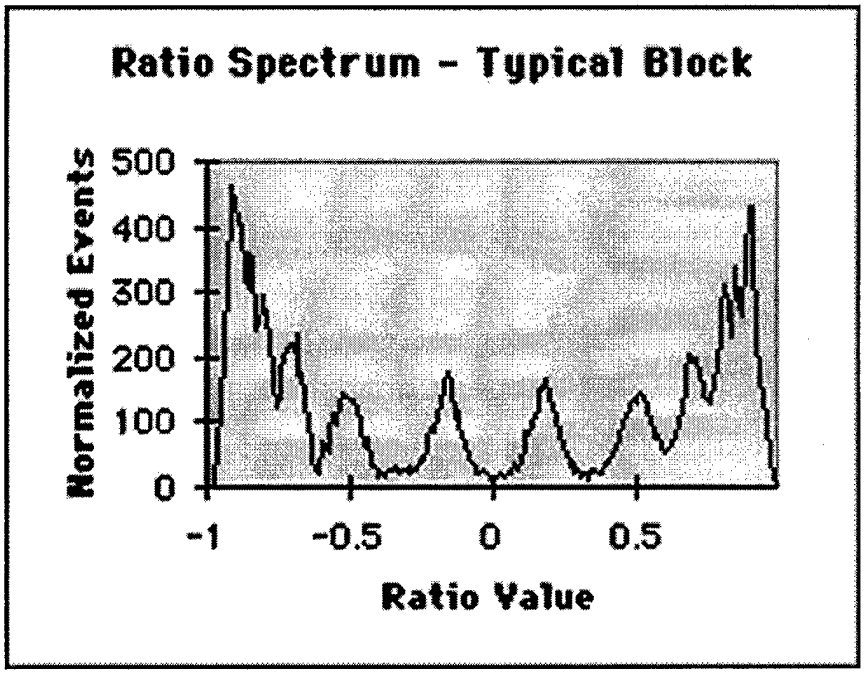

Figure 8: Normalized difference Spectrum from a Typical Block Measured with ^{68}Ge.Photofractionevents. Note that the outer crystals are not fully resolved in this block consisting of twelve 1mm crystals.

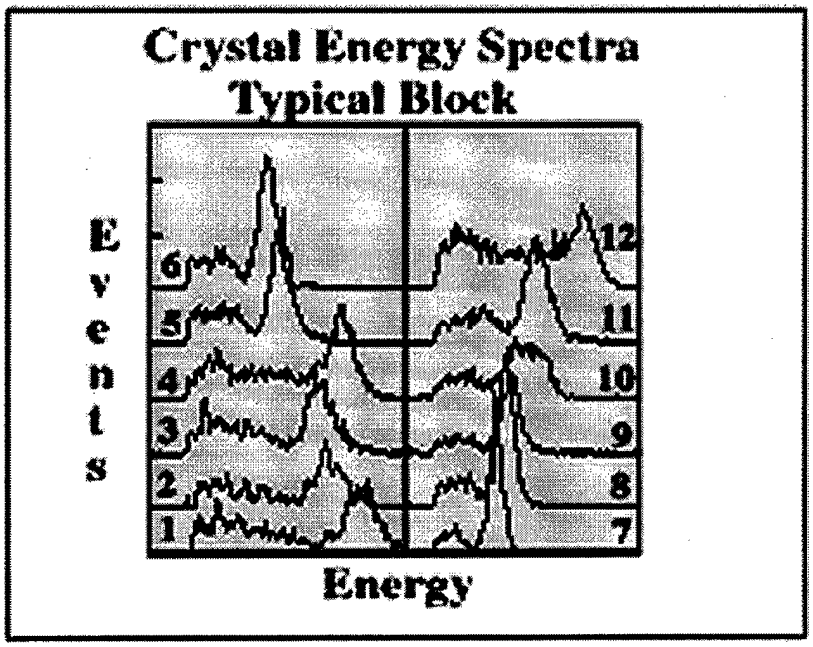

Figure 9: Energy spectra measured from a typical block using a ^{68}Ge source. Crystal numbers within the block are indicated at the sides.

E. - Software Design:

In order to collect, reconstruct and display PET data, a number of software modules are necessary. Our approach has been to develop software for the prototype device using C/C_{++} code in the DOS operating system. Modules for the following functions have been written and are operational: data acquisition; data preprocessing (i.e., identification of valid events and production of a sinogram data set for reconstruction); correction for sensitivity variations; image reconstruction analysis and display. Work is currently underway to adapt them to Windows95/98 graphical interfaces using Visual C_{++} 6.0 and MATLAB. Also, writing various modules for physical corrections needed to produce quantitative images is just beginning. Such corrections include photon prompt scatter, accidental coincidences, radioactive decay and dead time. The preprocessing program which produces the image sinogram has been benchmarked in several modern (300-500 Mhz) processors under the Windows95 operating system. Event processing, with non-optimized code takes approximately 7.5 microseconds on a 400 Mhz computer.

This should allow coincidence event rates to exceed 100,000 /sec without being limited by event processing time.

F. - Studies on the Prototype Instrument:

A photograph of the prototype is shown in figure 10. Some of he most important parameters to be considered in a PET system are the spatial resolution, sensitivity, countrate capability, field uniformity, and ability to reproduce radioactivity concentrations over a wide dynamic range. Physical measurements of these parameters have been made on the prototype. Examples of the results are presented in figures 11-15 and tables 1 and 2 and are discussed below.

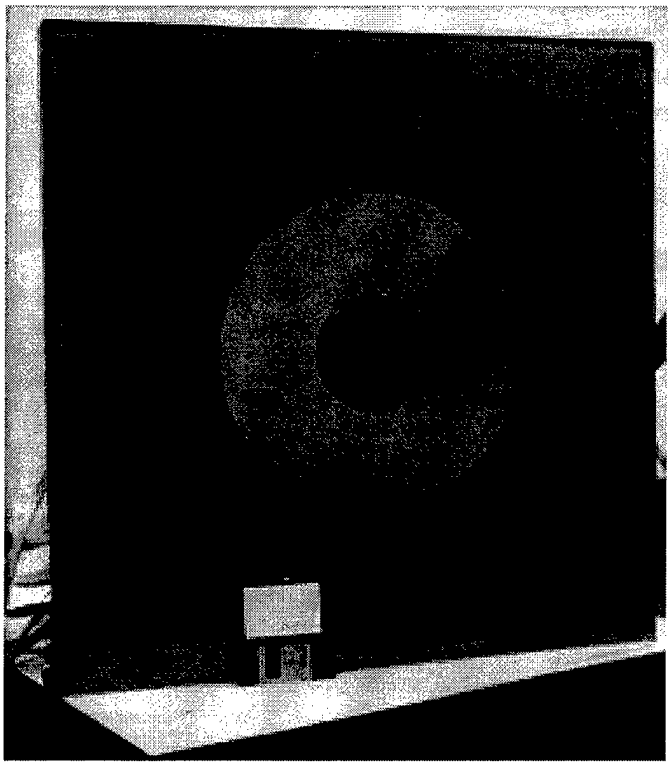

Figure 10: Photograph of 12 cm diameter prototype with 5 cm imaging aperture. A 3.5 inch disk is shown for scale.

Figure 11 shows a reconstructed image of 6 "point" sources of ^{18}F radioactivity which consist of 0.4mm i.d. needles placed perpendicular to the imaging plane spaced radially at 5mm intervals starting at the field center. Table 1 summarized the resolution measured at each position (resolution is full width at half maximum of a profile through the center of each source). At the enter the resolution is 1.25mm and degrades to 1.6mm at 2.5cm radius

due to the detector penetration effects discussed above. However, within a central circle of about 1.75cm radius only minimal degradation is observed. The axial resolution (or effective imaging plane thickness) at the center of the field was measured by moving a point source of ^{18}F axially through the field in 0.1mm steps. It should be noted that the axial resolution can be reduced by narrowing the gap in the Pb collimators which define the imaging gap at a sacrifice of sensitivity that is inverse to the square of the reduction. Figure 12 shows an alterative measure of resolution. Images of small squares of plastic which have arrays of ^{18}F-filled wells of various diameters and separations are shown. The smallest set, 1.5mm diameter with 2.5mm separation, are completely resolved.

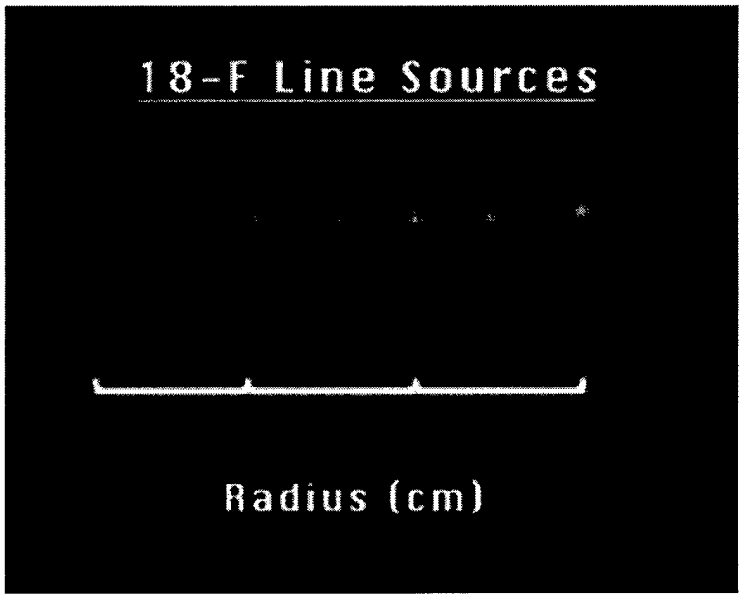

Figure 11: Reconstructed Image of six 0.4mm ^{18}F line sources 0.5 cm apart. The scale shown is at 1 cm intervals and center of the image is at the center of the field.

Table 1: Spatial Resolution at Various Field Radii Measured from the 0.4mm Diameter Line Sources of figure 10. Axial Resolution was measured by moving a point source of ^{18}F through the field in 1 mm steps. Full Width at Half Maximum(FWHM) and Full Width at Tenth Maximum(FWTM) for each source.

RADIUS (cm)	FWHM (mm)	FWTM (mm)
0	1.25	2.45
0.5	1.23	2.50
1.0	1.30	2.60
1.5	1.35	2.60
2.0	1.61	3.0
2.5	1.72	3.0
Axial(Center)	1.8	3.4

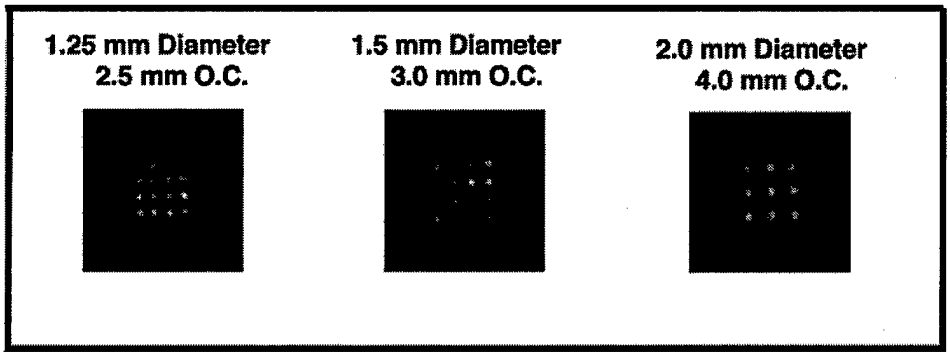

Figure 12: Reconstructed images of 1x1x0.75 cm high polystyrene cubes having ^{18}F-filled wells. The well diameters and separations are indicated.

The system sensitivity was measured using cylindrical sources of ^{18}F radioactivity of varying diameter and a point source of ^{18}F at the center of the field. The sensitivity as measured here represents all coincidence events above a 125 keV threshold. The corresponding computed sensitivities determined form the Monte Carlo simulations agree fairly well with the measurements as shown in table 2.

Table 2: Measured sensitivity for cylindrical objects of varying diameter and for a point source at the field center. The measurements include all events above 125 keV. Monte Carlo simulation results are shown for comparison.

Source Diameter (cm)	Measured Sensitivity (cps/uCi/cc)	Computed Sensitivity (cps/uCi/cc)
0.5	3	-
2.0	40	52
2.5	69	86
3.5	145	162
4.5	204	230
Point	30 cps/uCi	70 cps/uCi

Figures 13a and b show measurements of the system's response to a range of radioactivity concentrations in small objects. A test object consisting of five 2.7mm diameter cylinders containing various concentrations of ^{18}F radioactivity in a 3.5cm diameter water absorber was imaged as shown in figure 13a. The measurement was then repeated over several ranges of radioactivity and relative radioactivity concentrations in the small cylinders measured from the reconstructed images. Figure 13b shows a plot of PET measured radioactivity concentration versus actual concentration measured by well counter along with a linear least squares fit to the experimental points.

Figure 14 shows the countrate performance of the prototype measured with a 3cm diameter cylindrical source of ^{13}N radioactivity. The plots show the behavior of the whole system single events, coincidence events and accidental coincidences as well as the singles-to-trues ratio as a function of time. Since the 13N source is decaying with a 10 minute half-life, the time axis is equivalent to decreasing radioactivity concentration over a dynamic range of 256 to 1. The system shows little effect due to deadtime of the front-

end electronics up to coincidence rates of 100,000 events/second.

Figure 15 shows a measurement of reconstructed field uniformity. The relative radioactivity concentration was measured in 123 circular regions of 3.5mm diameter distributed uniformly over the reconstructed image of a 3.5cm diameter cylinder of ^{18}F radioactivity. The figure shows a plot of the signals from these regions with error bars that represent the sample standard deviation. It should be noted that the expected standard deviation for 3.5mm regions in this 3M event image due to measurement statistics alone is approximately 2.5% on average, while the measured sample standard deviation, including the effects of non-uniformities is 5.5%

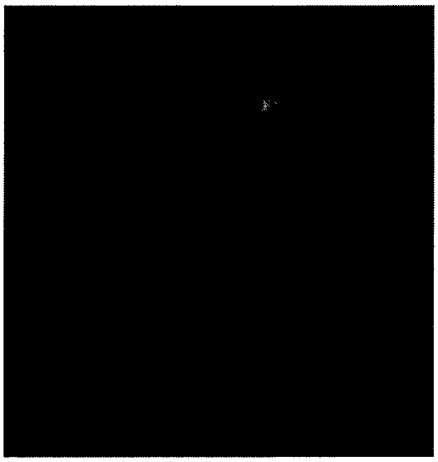

Figure 13a: Reconstructed image of five 2.7 mm diameter cylinders containing ^{18}F placed in a circular water absorber of 3.5 cm diameter. The cylinders are placed 1.5 cm radially from the center of the field and the dynamic range of the radioactivity concentrations is approximately 5 to 1.

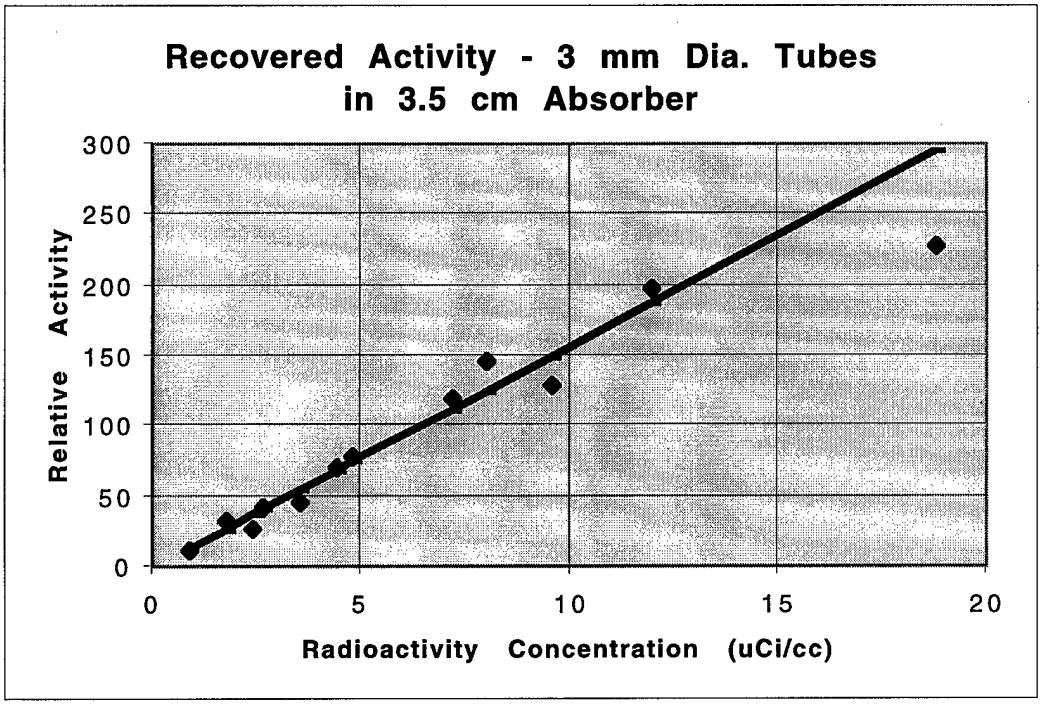

Figure 13b: Reconstructed radioactivity concentration in 3mm cylinders as versus known concentration. A linear least squares fit to the data is also shown.

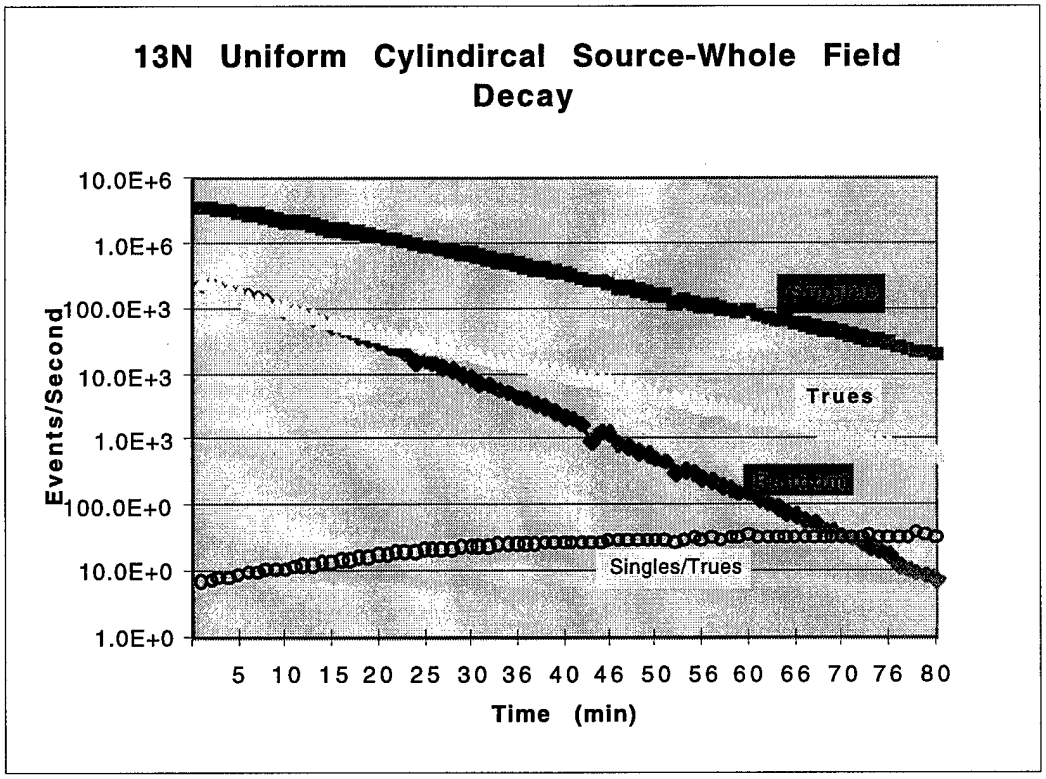

Figure 14: Whole-field single events, accidental coincidences, true coincidences and singles/trues ratio measured with a decaying ^{13}N cylindrical source 3.5 cm in diameter.

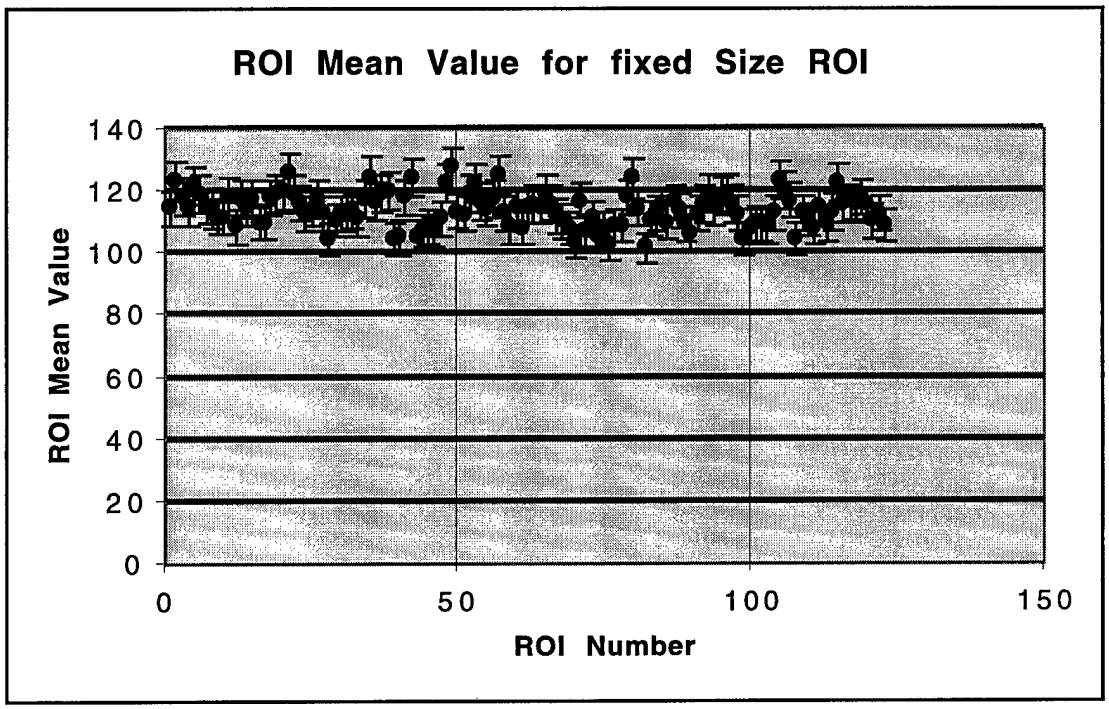

Figure 15: Uniformity of reconstructed 3.5cm diameter cylinder of radioactivity measured from a uniform sampling of 3.5 mm diameter circular regions. Error bars are sample standard deviation.

The overall conclusions that may be drawn from the above described measurements are as follows:

1. The best system resolution is 1.25mm rather than the 1 mm expected based on system design. This may be explained by the relatively poor identification of the outer crystals in the blocks, the presence of small alignment errors in the crystals and poor energy resolution at the center of the blocks due to poor light collection.
2. The overall sensitivity is in fairly good agreement with simulation results although the measured results are systematically lower.
3. The recovery of radioactivity is linear over a wide range of concentrations from 05.-18uCi/cc.
4. The central field region is uniform to less than 5%.
5. The system support countrates up to 100,000 coincidences per second with little front-end deadtime. The more practical limit of random coincidences comprising more than half the signal is reached at about 70k total coincidences/sec, well below the rates where deadtime becomes significant.
6.

A summary of the performance characteristics of the prototype device is given in table 3.

Table 3: Specifications of 12 cm Diameter Prototype PET Instrument

PARAMETER	VALUE
Number of Planes	1
Detector Array Diameter	12 cm
Number of Crystals/Type	360/LSO
Crystal Dimensions	1 x 4.5 x 5mm
Number of Phototubes/Blocks	30
In-Plane Spatial Resolution	1.2 mm center - 1.6 mm at 2.5cm
Axial Resolution	0.25 - 0.5 mm
Field of View	8 cm
Point Source Sensitivity	30 coincidences/second/uCi
Field Uniformity	< 5% variation in 3.5 cm disk
Randome=Trues	70000 conic./sec

G. - Preliminary Studies for Synthesis of PET Compounds:

To-date a survey of possible tetracycline compounds and bis-phosphonate compounds has been made in order to determine which are most easily labeled with ^{11}C and ^{18}F. Several synthesis routes have been established. Also, the possibility of using longer-lived ^{124}I, which is also a positron emitter, as a radioactive label has also been studied. In the past ^{124}I has not been readily available but our laboratory has undertaken to set up a production facility for this isotope under separate funding.

H. - Design for Primate and Human arm Imaging:

Based on the simulation, computational and experimental studies carried out a design for the device to be constructed for bone imaging has been generated. The main features of the design are given in Table 4. The main differences from the prototype in addition to a newly designed preamplifier are:

1. Wider LSO crystal elements, 1.2 mm rather than 1, to give better block performance at 1.2mm resolution.
2. 14.5cm detector array diameter.
3. Longer LSO crystal elements to improve sensitivity. 7mm rather than 5mm.
4. More phototube channels, 36 rather than 30 to accommodate the larger diameter.
5. Windows 95/98-based data acquisition interface which consists of a PCI data channel and a FIFO buffer to eliminate interface dead time.
6. Software running through graphical interfaces under Windows.
7. Corrections for deadtime, accidental coincidences and scattered photons leading to full quantitation.

In addition, we have designed a moving mechanical arm support which will be operated under computer control and integrated with the data acquisition software. The parts have been ordered for this device and the computer interface and control software are currently being completed.

Table 4: Specifications of 15 cm Diameter PET Instrument

PARAMETER	VALUE
Number of Planes	1
Detector Array Diameter	14.5 cm
Number of Crystals/Type	360/LSO
Crystal Dimensions	1.25 x 5 x 7mm
Number of Phototubes/Blocks	36
In-Plane Spatial Resolution	1.25 mm center - 1.6 mm at 3cm
Axial Resolution	0.25 - 0.5 mm
Field of View	8 cm
Point Source Sensitivity	50 coincidences/second/uCi/cc
Field Uniformity	< 3% variation in 4.5 cm disk
Randome=Trues	60000 conic./sec

I. - KEY RESEARCH ACCOMPLISHMENTS:

1. Demonstration of the feasibility of very high resolution PET imaging in small scale objects.
2. Construction of a working prototype of a small-scale PET instrument which achieves resolution approaching 1 mm. To our knowledge this is the highest resolution PET device in existence at this time.
3. Specification of a PET instrument for the imaging of extremities and beginning of construction.

J. - REPORTABLE OUTCOMES:

A number of the studies carried out during this grant period are reportable in fact some have already been published. These include:

1. Feasibility of 1 mm PET imaging (published).
2. Simulation of small scale PET geometries and detector properties (unpublished).
3. Performance evaluation of a small scale PET instrument (accepted by 1999 IEEE Medical Imaging Conference, MS in preparation).

Please see appendix for details of the published work.

K. - CONCLUSIONS:

During the first year of the project we have established a design for a high resolution PET instrument for bone imaging. The design is based on simulation studies of PET detector and system properties, benchtop experiments with detector elements and electronic circuit designs, the construction and evaluation of a prototype imaging device as an experimental verification of feasibility. The main conclusion from this work is that it is feasible to carry out small-scale PET imaging at resolutions approaching 1mm.

The output of the work in relation to the project goals are detector block design processing circuit board designs and software development all of which will be used in the instrument to be built for primate bone imaging. We have begun ordering components for this and will begin mechanical assembly within the next month, this is approximately on time according to our proposed work scope.

Very high resolution PET imaging is the only technique currently available which could be used for the bone growth studies in-vivo will be begun during the last few months of

the second year of the project. Very high resolution PET imaging is likely to have application in many other areas as well. The most exciting, perhaps, is the measurement of various physiological and biochemical parameters in mice. Genetically-altered-mouse-based disease models are becoming widely used for the study of abnormal physiology and the very high resolution offered by the instruments developed in this project is ideal for imaging them.

L. - APPENDIX:

1. Development of a Small Animal Pet Imaging Device with Resolution Approaching 1mm", JA Correia, CA Burnham, D Kaufman, AJ Fischman, J Nucl Med 40:285P (1999) Abstr.

2. Development of a Small Animal Pet Imaging Device with Resolution Approaching 1mm", JA Correia, CA Burnham, D Kaufman, AJ Fischman, IEEE Trans Nucl Sci 46:631-635 (1999) (Reprint enclosed).

3. A Pet Imaging Instrument for High Resolution Rat and Mouse Imaging ", JA Correia, CA Burnham, D Kaufman, E. Carter, AL Brownell, AJ Fischman, Accepted for presentation at "High Resolution Imaging in Small Animals with PET, MRI and other Modalities", Amsterdam, Sept 1999 (abstract enclosed)

4. Performance of a Small Animal Pet Imaging Device with Resolution Approaching 1mm", JA Correia, CA Burnham, D Kaufman, AJ Fischman, accepted for presentatiom, IEEE Nuclear Science Symposium and Medical Imaging Conference, 1999, Manuscript in preparation (not included)

TIME IMAGE GUIDED BIOPSY -
A DUAL SLANT-ANGLE
OLID STATE GAMMA CAMERA.
zzuoli, M. Kipper, I. Khalkhali, W.
ifornia at San Diego Medical Center,
ospital, Vista, CA; Harbor-University
les Medical Center, Torrance, CA;
iego, CA. (335)

y collimator was mounted on a solid-state
Imager™). The 21.6 x 21.6 cm (approx.
lit into two halves, each viewing the same
l (parallel) holes. The resulting 60-degree
multaneous stereoscopic views of one or
it of the collimator face. A relatively weak
a breast phantom to simulate radioactiv-
of Tc-99m was placed in the tip of a nee-
opsy needle. The phantom was positioned
rtically) and the operator. Radioactivity in
on the monitor. By advancing the needle
he needle tip could be guided to the lesion.
tip was guided to within 3mm of the le-
of the needle tip and lesion were super-
had no trouble guiding the needle tip
/out) of the needle tip was determined by
f the needle were lateral, i.e., needle not
o deep, to the dual images of the lesion.
ime needle guidance should be possible
tor system. Its primary use may be when
raphically, yet concentrates a radiophar-
Possible applications include guide-wire
ization for injecting sulfur colloid into the
tion, and stereotactic breast biopsy under

one at regular QC. **Conclusions**: The method proved to be valuable in acceptance tests and regular QC. It is sensitive and produces full FOV maps of HAE. Errors ≥0.25° are detectable and were observed in several collimators.

No. 1258

DEVELOPMENT OF A SMALL ANIMAL PET IMAGING DEVICE WITH RESOLUTION APPROACHING 1MM.

J. A. Correia*, C. A. Burnham, D. Kaufman, A. J. Fischman, Massachusetts General Hospital, Boston, MA. (500477)

Small animal imaging presents a situation where positron range effects and sampling are the dominant physical limitations to spatial resolution. Annihilation-pair non-colinearity and scatter are minimized due to the small dimensions of both instrument and subject. Theoretical and simulation studies support the idea that spatial resolution on the order of 1mm can be achieved with ^{18}F and ^{11}C. The availability of LSO as a scintillator material for PET makes possible the design of detector modules with resolution approaching one millimeter. The purpose of the work reported here was to design and construct a prototype single-plane, high resolution PET instrument using LSO detectors. The approach taken was to develop a simple prototype that maximizes the use of software data processing to minimize electronics construction. The detector array consists of a single ring of 360 1x4.5x5 mm LSO crystals organized into blocks of 12 crystals each viewed by two photomultipliers. To achieve high resolution, thin crystals (5 mm) are used for several reasons; first, the use of thin crystals moderates the degradation and non-uniforminty of resolution caused by multiple detector penetration at photon incidence angles far from the normal, and secondly, blurring due to multiple interaction sites is reduced. The choice of thin crystals represents a sacrifice in sensitivity to preserve resolution. The system is also operated with a low energy threshold to maximize the number of single-interaction-site events. Crystals are identified using two block-specific lookup tables, one applied to the normalized pm tube differences and one applied to the total block energy. Reconstructed resolution was measured using 0.42 mm diameter 18F line sources. The resolution at the center of the field is 1.2 mm and the radial resolution at 2.5 cm radius is 1.65 mm. System sensitivity was measured using cylindrical water-bath sources of various diameters yielding 1.2 cps/uCi/cc for a 0.5 cm source and 72 cps/uCi/cc for a 4.5 cm source. Imaging studies in rats and mice with ^{18}F- FDG and several ^{11}C receptor compounds have been begun.

Development of a Small Animal PET Imaging Device with Resolution Approaching 1mm

J.A. Correia, C.A. Burnham, *Senior Member IEEE,* D. Kaufman, A.J. Fischman
Massachusetts General Hospital, and Harvard Medical School, Boston, MA 02114

Abstract

The work presented here describes progress in the design and construction of a single-plane PET tomograph having spatial resolution approaching 1 mm. The system consists of a 12 cm diameter ring with 360 LSO detectors viewed by 30 photo-multiplier tubes. Thin (5 mm) crystals and a low energy threshold are used. Crystals are identified using both position arithmetic and energy criteria. To-date the system construction has been completed, system tuning carried out and imaging studies begun.

I. INTRODUCTION

Positron emission tomography (PET) has achieved major successes during the past ten years as a metabolic imaging modality, especially in human and large animal subjects. Instrumentation for use in these regimes has become highly developed and reliable and is used routinely in many laboratories throughout the world. Recently, a number of workers have designed and successfully constructed instruments which image at higher resolution over small-scale fields, with the goal of imaging small animals such as monkeys, rats and mice [1-11].

Small animal imaging presents a situation where positron range effects and sampling are the dominant physical limitations. Annihilation-pair non-co-linearity and photon scatter are minimized due to the small dimensions of both instrument and subject. Theoretical and simulation studies support the idea that spatial resolution on the order of 1mm can be achieved with ^{18}F and ^{11}C [12-14]. The availability of LSO as a scintillator material for PET leads to several possible approaches to designing detector modules for PET systems having spatial resolution approaching one millimeter [15].

The purpose of the work reported here was to assess the feasibility of 1mm imaging by designing and constructing a prototype high resolution PET instrument using LSO detectors. The approach taken was to design and construct a simple prototype with as much flexibility as possible in hardware and software implementation. A simple design allows for straightforward modification and adaptation.

II. SYSTEM DESIGN

A. *General Design*

Simulation studies of the geometry including positron range, annihilation non-co-linearity and scatter have been used to develop the design presented here. The approach maximizes the use of software data processing to minimize electronics construction and maintain flexibility. A system block diagram is shown in figure 1.

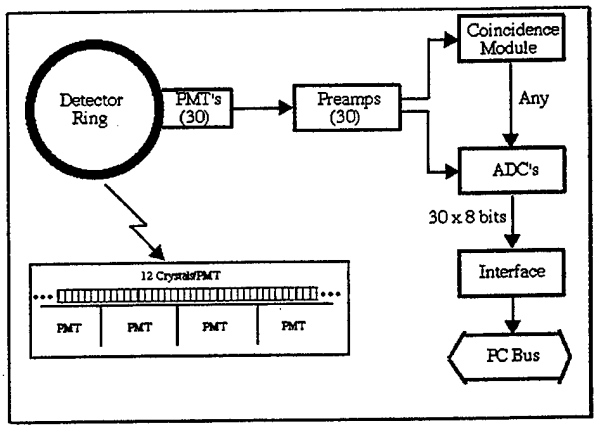

Figure 1: System Block Diagram

The detector array consists of a single ring of 360 1x4.5x5 mm LSO crystals organized into blocks of 12 crystals each viewed by two RCA 647 photomultipliers (PMT's) in a one dimensional implementation of the geometry proposed by Wong [16]. To achieve high resolution, thin crystals (0.5 cm) are used for several reasons; first, the use of thin crystals moderates the degradation and non-uniformity of resolution caused by multiple detector penetration at photon incidence angles far from the normal, and secondly, blurring due to multiple interaction sites is reduced [14]. The choice of thin crystals represents a sacrifice in sensitivity to preserve resolution.

The PM Tube signals are processed for timing and position. The coincidence logic uses the timing signal to identify any coincidence event from the central volume of the detector. The coincidence resolving time of the circuitry is 16 ns. The 30 linear position signals are DC coupled to the sample-and-hold ADC. Pulse shaping equivalent to single

0018-9499/99$10.00

delay line clipping is used. When a coincidence event is detected the 30 signals are simultaneously sampled and converted to thirty 8 bit words. The use of an 8 bit ADC is a compromise between speed and accuracy. The deadtime is limited by the time required to transfer, process and store an event in the computer. The sample update pulse interval is varied to minimize this deadtime. The preamplifiers, coincidence circuits and digital conversion circuits were implemented using standard logic elements. Provision has been made for direct and indirect estimation of random coincidences by measurement of triple coincidence and delayed coincidences.

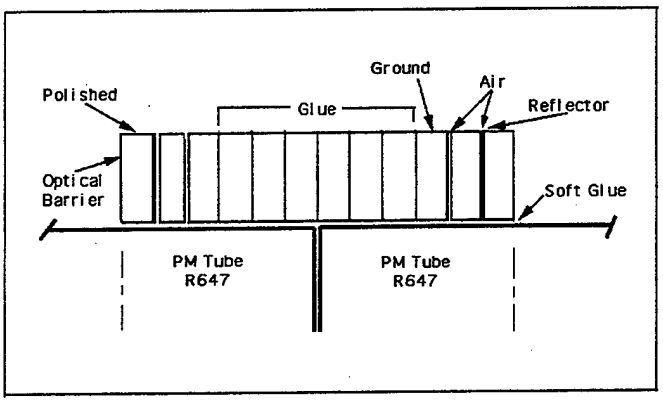

Figure 2. Detail of Block Design showing the various surface preparations used.

B. *Block Design*

The individual blocks were designed based on a combination of computer simulations and experimental measurements of the optics for various geometries. The eight interior crystal faces are glued together in a jig with an 8° taper in order to point them toward the ring center. The next two on each side are separated from central crystals and each other by an air gap. The two outside crystals have polished surfaces and a partial reflector isolates them from the adjacent crystals. A reflector is used between blocks. The average fractional signal from each of the crystals for 0.511 keV photons is shown in figure 3. Approximately 1/3 of the light from the peak signals is lost and the energy resolution of the blocks at 0.511 keV is 17% at the center.

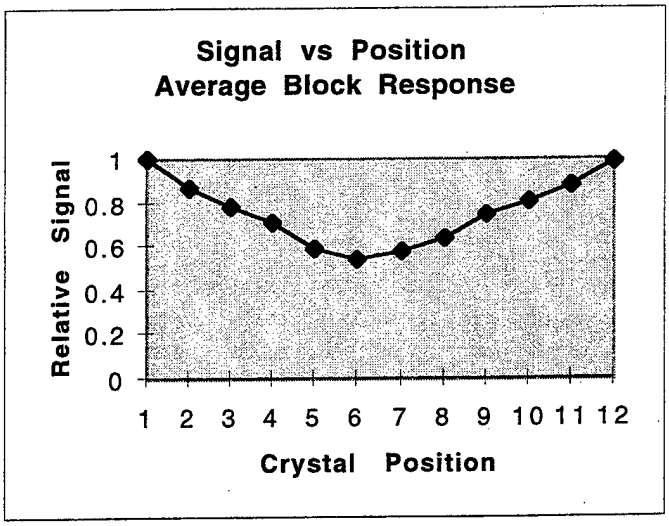

Figure 3: Measured relative crystal signal. Average over 30 blocks.

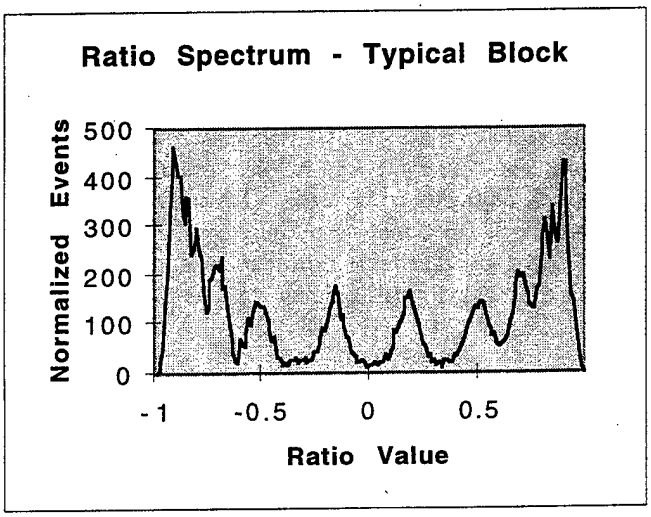

Figure 4.: Ratio from typical block measured with ^{68}Ge. Photofraction events.

C. *Signal Processing*

When a coincidence event is registered by the hardware, the 30 PMT signals are transferred to the computer. The sum of neighboring pairs of PMT signals is computed and if a sum exceeds both neighboring sums and an energy threshold, a block is identified. If three blocks are identified, a triple coincidence is recorded. When exactly two blocks are identified within a data set the processing proceeds to the identification of the individual crystals within each.

The normalized difference (**R**) of PMT signals (**A** and **B**) in each block is determined as follows:

$$R = (A - kB) / (A + kB) \quad (1)$$

and if an energy criterion to select only photopeak events:

$$E > E_{threshold} \quad \text{and} \quad E_{lower} < E < E_{upper} \quad (2)$$

is met, a particular crystal is identified, otherwise the event is rejected.

A plot of the **R** spectrum from a typical block is shown in figure 4. Figure 5 shows the average bounds for the 30 blocks and figure 6 the individual-crystal energy spectra from a typical block.

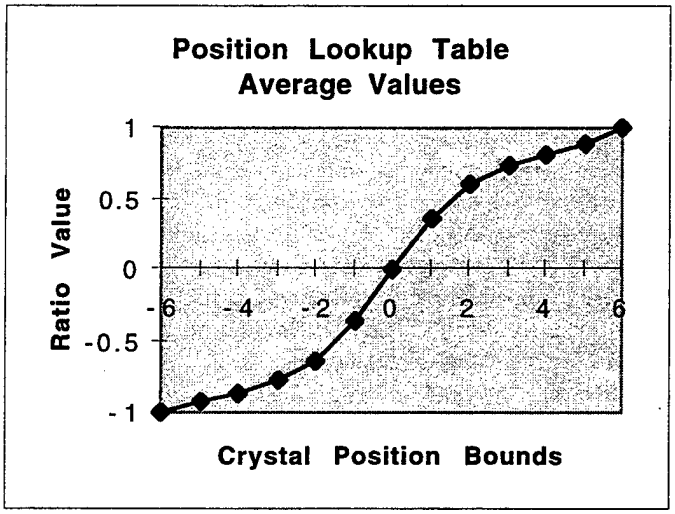

Figure 5: Measured ratios averaged over 30 blocks plotted as a function of ratio with crystal bounds indicated.

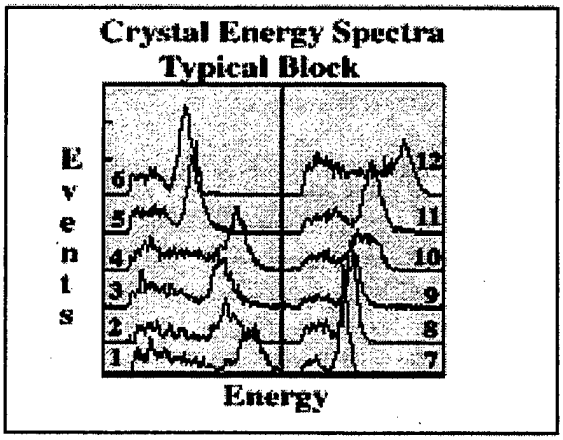

Figure 6: Energy spectra measured from a typical block using a ^{68}Ge source.

The PMT gains are adjusted such that the maximum signal of each utilizes the full dynamic range of the ADC. A gain correction (**k** in equation 1), implemented via a lookup table, is then applied in the **R** calculation to force the ratio at the center of each block to zero.

A given value of **R** is associated with an individual crystal within the block via a lookup table specifying the lower and upper levels of the ratio values for that crystal. A good event is recorded if the boundary conditions are met and the phototube-sum, or total energy, signal is within a window derived from the crystal energy spectra. Boundary and energy lookup tables are specified for each block to account for small variations in crystal properties and alignment. The determination of the lookup tables is an iterative process in which a starting set of boundaries are specified from **R** plots taken with wide energy windows, then a set of narrower energy windows are specified from the energy spectra and the process repeated until an optimum is reached.

Coincidence data are mapped to a sinogram format for storage, corrected for sensitivity, randoms and attenuation and reconstructed using a standard convolution-backprojection algorithm.

III. SYSTEM PERFORMANCE

Reconstructed resolution was measured using 0.42 mm diameter ^{18}F line sources (22 gauge needles). Reconstructions were done with a ramp filter having a cutoff frequency of 2 mm^{-1}. Figure 7 shows an example of these measurements and table 1 summarizes the results. The resolution at the center of the field is 1.25 mm and the radial resolution at 2.5 cm radius is 1.75 mm.

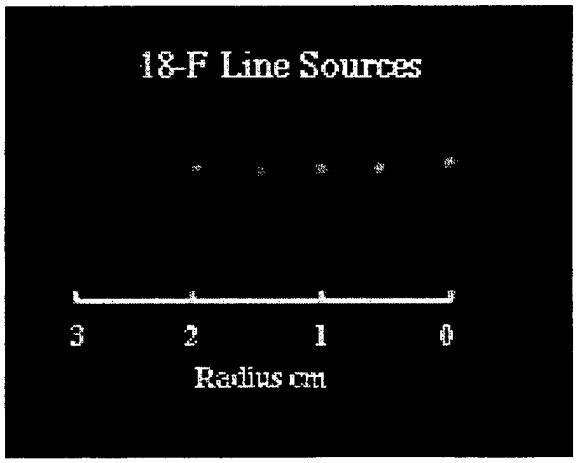

Figure 7: Reconstructed Image of six 0.4mm 18F line sources 0.5 cm apart. The scale shown is at 1 cm intervals with the field center at the right.

The axial resolution of the system at the center of the field was measured using a point source of ^{18}F stepped through the field in 0.1 mm steps. The axial resolution determined by this method was 1.8 mm for the results presented here. In general the axial resolution can be varied by adjusting the distance between two Pb collimator sections shielding the detectors. These collimators consist of two annuli of 5 cm inner radius and 12 cm outer radius. Each annulus is 6 cm long in the axial direction. In addition, the detector ring is shielded on both sides by a 1.25 cm annular Pb plate.

Table 1: Spatial Resolution at Various Field Radii Measured with 0.42 mm Diameter Line Sources.

RADIUS (cm)	FWHM (mm)	FWTM (mm)
0	1.25	2.45
0.5	1.23	2.50
1.0	1.30	2.60
1.5	1.35	2.60
2.0	1.61	3.0
2.5	1.72	3.0

System sensitivity was measured with a centrally located point source of ^{18}F, a ^{68}Ge pin source and uniform fields of various diameters containing ^{18}F. Each uniform field source was approximately 4 cm in z-extent. The results of these measurements are summarized in table 2. The sensitivity listed represents all true coincidences formed by events above a 150 keV energy threshold.

Table 2: Measured sensitivity for cylindrical objects of varying diameter. The reported sensitivity includes all events above 150 keV. The point source sensitivity was measured with an ^{18}F point and is given in units of cps/uCi.

Diameter (cm)	Sensitivity (cps/uCi/cc)
0.5	3
2.0	40
2.5	69
3.5	145
4.5	204
Point	30 cps/uCi

Preliminary studies in rats have been begun as a means of testing the performance of the instrument under actual laboratory conditions. To-date, only imaging studies at low countrates have been carried out. Figure **8** shows three coronal images of a rat brain after injection of 4 mCi of ^{18}F-FDG. The collection time for each image data set was approximately twenty five minutes.

Figure 8: Coronal slices, 1.8 mm thick, in rat brain after injection of 4 mCi ^{18}F-FDG. A: 1 M events. Location: 15 mm forward of inter-aural line. High-uptake structures are the tips of the olfactory bulbs. B: 2.5 M events. Location: 10 mm forward of inter-aural line showing cerebral cortex and striatum. C: 1.0 M events. Coronal image of the posterior of the brain.

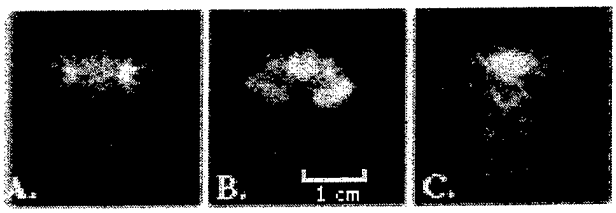

IV. CONCLUSIONS

The possibility of PET imaging with LSO detectors at resolution approaching 1 mm has been demonstrated in a prototype single-plane instrument. Resolution degradation is moderated by the use of thin crystals to the degree that objects up to approximately 3.5 cm diameter show only minimal degradation and objects up to approximately 5 cm in diameter maintain off-center resolution below 2 mm. The sensitivity of the instrument described here is low due to two factors. The first is the use of thin detectors for the reasons stated above and the second is the need to limit events in a given crystal to a range of energies about the photopeak due to poor light collection from the center of the blocks. This process reduces the efficiency for useful events by 40-60% depending on the energy window-widths chosen.

The measurements of spatial resolution using 0.45 mm diameter needles did not yield 1 mm resolution as at the center of the field as dictated by sampling. This is due in part to poor spatial resolution at the ends of some blocks. This loss of resolution accounts for the fact that the measured resolution is uniform over the central region of the field.

The wide range of signal amplitudes led to poor timing and sensitivity at the centers of some blocks. This effect has not been addressed to-date. Nevertheless the instrument may be effectively used for static imaging situations such as FDG imaging with moderate injected doses and may be useable, with larger injected doses, for some receptor studies. Preliminary tests of the instrument have been carried out in rat brain. The most effective use of this instrument in the future however is expected to be in imaging mice.

Ongoing work includes characterization and refinement of the detector-block design, crystal identification and time discriminator logic. Refinements of corrections for other physical effects such as field non-uniformity, attenuation, scatter and randoms in the projection data are also being

developed. A multiple ring version of this instrument with somewhat larger detector-ring diameter is currently being designed.

V. ACKNOWLEDGMENT

This work was supported in part by Department of Defense Grant # USAMRAA-DAMD17-98-8511.

VI. REFERENCES

[1] Del Guerra A, Scandola M and Zavattini G, "YAP-PET: First Results of Small Animal Positron Emission Tomograph Based on YAP:CE Finger Crystals." *IEEE Transactions on Nocl. Sci.,* 45:3105-3108, 1998.

[2] Pichler B, Boning G, Lorenz E, et. al., "Studies with a Prototype High Resolution PET Scanner Based on LSO-APD Modules", *IEEE Transactions on Nucl. Sci.* 45: 1298-1302, 1998.

[3] Cherry SR, Shao Y, Silverman RW, et. al. , "Micropet: a high resolution PET Scanner for Imaging Small Animals, *IEEE Transactions on Nucl. Sci.*, 44:1161-1166, 1997.

[4] Weber S, Terstegge A, Engels R, et al, The KFA TierPET: Performance characteristics and measurements." *IEEE Nuclear Science Symposium & Medical Imaging Conference Record,* 1117-1120, 1997.

[5] Watanabe M, Okada H, Shimaza K, et. al., A high resolution animal PET scanner using compact PS-PMT detectors, *IEEE Transactions on Nucl. Sci.* 44: 1277-1282, 1997.

[6] Bruynodonckx P,Xuan l, Tavernier S, Zhang S, "Perforemance of a small animal PET scanner based on photosensitive wire chambers, "*IEEE Nuclear Science Symposium & Medical Imaging Conference Record,* 11335-1340, 1997.

[7] Moses WW, Virador SE, Derenzo SE, et al, "Design of a High-Resolution, High-Sensitivity PET Camera for Human Brains and Small Animals." *IEEE Transactions on Nucl. Sci.*, 44:1487-1491, 1997.

[8] Lecompte R, Cardorette J, Rodrique S, et. al."Initial Results from the Sherbrooke Avalanche Photodiode Positron tomograph", *IEEE Transactions on Nucl. Sci.* 43:1952-1957, 1996.

[9] Bloomfield PM, Rajeswaran S, Spinks T,et. al., "The design and Physical Characteristics of a Small-Animal Positron Emission Tomograph", *Physics in Med. and Biol.,* 40:1105-1196, 1995.

[10] Seidel J, Gandler WR, Green MV, "A Very High Resolution Single Slice Small Animal PET Scanner Based on direct Detection of Coincidence Line Endpoints", *Journal of Nucl. Med.* 35:p 40P, 1994.

[11] Tavernier S, Bruyndonckx P and Zhang S, "A fully 3D small PET scanner.", *Phys. Med. Biol.,* 37: 635-643, 1992.

[12] Correia JA, Burnham CA , Kaufman D, et. al, "Small Animal PET imaging Device - Preliminary Design Study", *J. Nucl. Med.* 38:44P, 1997

[13] Burnham CA., Elliott JT., Kaufman D., Chesler DA., Correia JA and Brownell G.L, "Single Interaction PET Detectors.' *IEEE Transactions on Nucl Sci,* 37:832-835, 1990.

[14] Burnham C A, Kaufman D E, Chesler D A, Stearns C W, Correia J A, Brownell G L: "A low-Z PET detector", *IEEE Transactions on Nucl Sci* . 37:832-834, 1990.

[15] Melcher C.L. and Schweitzer J.S, "Cerium doped lutetium oxyorthosilicate: A fast, efficient new scintillator." *IEEE Transactions on Nucl. Sci.* , 39:502-505, 1992.

[16] Wong WH, Uribe J, Hicks K, et al, "A 2-dimensional detector decoding study om BGO arrays with quadrant sharing photomultipliers." *IEEE Transactions on Nucl. Sci.* NS41: 1453-1457, 1994.

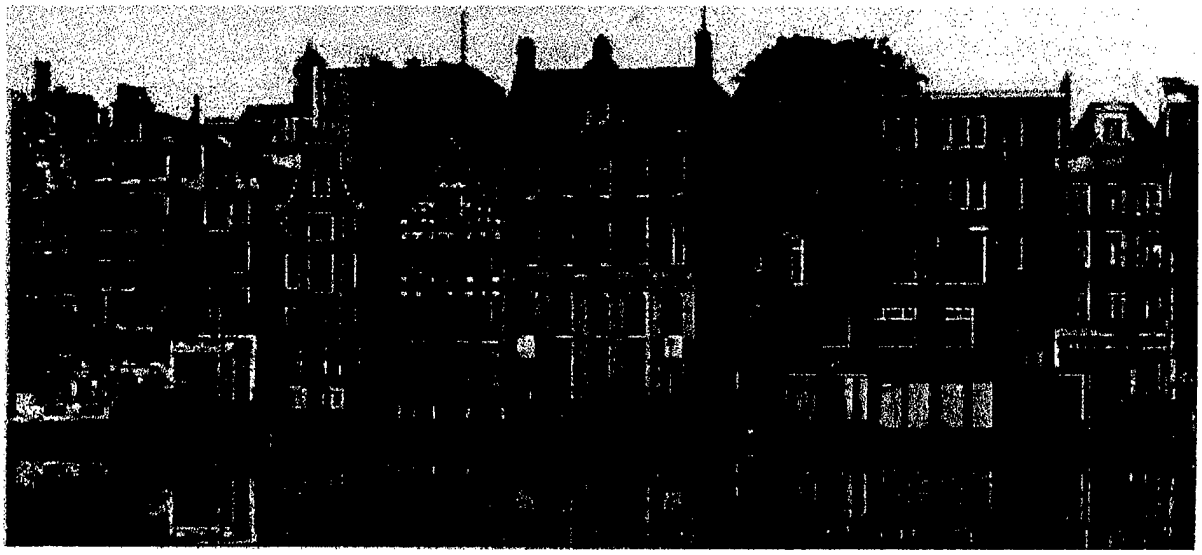

HIGH RESOLUTION IMAGING IN SMALL ANIMALS WITH PET, MR AND OTHER MODALITIES

INSTRUMENTS AND APPLICATIONS IN MODERN BIOMEDICAL RESEARCH

SEPTEMBER 27-29, 1999

ACADEMISCH ZIEKENHUIS VRIJE UNIVERSITEIT

AMSTERDAM, THE NETHERLANDS

Visit the **HiRes** website for information regarding program content, abstract submission, registration and hotel accommodations

http://www-HiRes.cc.nih.gov/HiRes

or request information by e-mail:

HiRes@nih.gov

by fax: **+1-301-496-0114**

or mail: HiRes
Room 1C401, Building 10,
National Institutes of Health
Bethesda, MD 20892-1180, USA

ORGANIZED BY

ACADEMISCH ZIEKENHUIS VRIJE UNIVERSITEIT, AMSTERDAM
TECHNISCHE UNIVERSITÄT MÜNCHEN
CRUMP INSTITUTE FOR BIOLOGICAL IMAGING, UCLA, LOS ANGELES
NATIONAL INSTITUTES OF HEALTH, BETHESDA

A PET Imaging Instrument for High Resolution Rat and Mouse Imaging

J.A. Correia, C.A. Burnham, D. Kaufman, E. Carter, A. Brownell and A.J. Fischman
Massachusetts General Hospital, and Harvard Medical School, Boston, MA 02114

Corresponding Author:
John A. Correia
Massachusetts General Hospital
Department of Radiology
32 Fruit Street
Boston, MA 02114
USA
PHONE: 617-726-8336
FAX: 617-726-5123
EMAIL: correia@petw6.mgh.harvard.edu

The current frontier in PET instrumentation lies at devices which image at higher resolution over small-scale fields, with the goal of imaging small animals such as monkeys, rats and mice. Small animal imaging presents a situation where positron range effects and sampling are the dominant physical limitations. Annihilation-pair non-colinearity and photon scatter are minimized due to the small dimensions of both instrument and subject. The availability of LSO as a scintillator material for PET leads to several possible approaches to designing detector modules for PET systems having high spatial resolution. The purpose of the work reported here was to design, construct and apply a prototype PET instrument with resolution approaching 1mm using LSO detectors. The approach taken was to design and construct a simple single-plane instrument with as much flexibility as possible in hardware and software implementation. A simple design allows for straightforward modification and adaptation.

The detector array consists of a single ring of 360 1x4.5x5 mm LSO crystals organized into blocks of 12 crystals each viewed by two photomultipliers. Each phototube views two blocks. Thin crystals (0.5 cm) are used to moderate the degradation and non-uniformity of resolution caused by multiple detector penetration at photon incidence angles far from the normal, and minimize blurring due to multiple interaction sites. The choice of thin crystals represents a sacrifice in sensitivity to preserve resolution. The PM Tube signals are processed for timing and position. The coincidence logic uses the timing signal to identify any coincidence event from the central volume of the detector. The 30 linear position signals are DC coupled to the sample-and-hold ADC. Pulse shaping equivalent to a single delay line clipping is used. When a coincidence event is detected the 30 signals are simultaneously sampled and converted to thirty 8 bit words. The deadtime is limited by the time required to transfer, process and store an event in the PC. The preamplifiers, coincidence circuits and digital conversion circuits were implemented using standard logic elements.

The individual blocks were designed based a combination of computer simulations and experimental measurements of the optics for various geometries. The eight interior crystal faces are glued together in a jig with an 8° taper in order to point them toward the ring center. The next two on each side are separated from central crystals and each other by an air gap. The two outside crystals have polished surfaces and a partial reflector isolates them from the adjacent crystals. A reflector is used between blocks. Approximately 1/3 of the light from the peak signals is lost and the energy resolution of the blocks at 0.511 keV is 17%.

Individual crystals are identified using three look-up tables customized for each block. These tables determine if the value of the normalized phototube difference and the energy of the event fall within defined ranges. The third table specifies a normalization factor to adjust for phototube gain differences.

The in plane spatial resolution of the device has been measured to be 1.2 mm at the field center, 1.27 mm at 1 cm radius and and 1.55 mm at 2 cm radius using 0.4 mm diameter line sources of 18-F. The axial resolution is variable but has been operated to date at 1.8 mm. The point source sensitivity for a source at the field center has been measured to be 30 coincidences/sec/uCi using an 18-F point source.The instrument has been applied to the imaging of adult rat brain, juvenile rat torso and adult mouse brain and torso using 18F FDG and fluoride ion as well as several 11-C labeled neuro receptor compounds.

The possibility of PET imaging with LSO detectors at resolution approaching 1 mm has been demonstrated in a prototype single-plane instrument. Resolution degradation is moderated by the use of thin crystals to the degree that objects up to approximately 3.5 cm diameter show only minimal degradation and objects up to approximately 5 cm in diameter maintain off-center resolution below 2 mm. The sensitivity of the instrument is low due to the use of thin detectors to preserve resolution and the need to limit events in a given crystal to a range of energies about the photopeak due to poor light collection from the center of the blocks. This process reduces the efficiency for useful events by 30-60% depending on the energy window-widths chosen.

The most effective use of this instrument in the future is expected to be in imaging mice. Future plans include the characterization and refinement of the detector-block design, further characterization of crystal identification and time discriminator logic, corrections for other physical effects such attenuation, scatter and randoms in the projection data and design of a multiplane device.